1 **Six-year source apportionment of submicron organic aerosols from near-**

2 **continuous highly time-resolved measurements at SIRTA (Paris area, France)**

3 Yunjiang Zhang[1,2*], Olivier Favez[1*], Jean-Eudes Petit[2], Francesco Canonaco[3], Francois Truong[2], Nicolas

4 Bonnaire[2], Vincent Crenn[2†], Tanguy Amodeo[1], Andre S.H. Prévôt[3], Jean Sciare[2,4], Valerie Gros[2],

5 Alexandre Albinet[1]

7 [1]Institut National de l'Environnement Industriel et des Risques, Verneuil-en-Halatte, France

8 [2]Laboratoire des Sciences du Climat et de l'Environnement, CNRS-CEA-UVSQ, IPSL, Université

9 Paris-Saclay, Gif-sur-Yvette, France

10 [3]Laboratory of Atmospheric Chemistry, Paul Scherrer Institute, Villigen PSI, Switzerland

11 [4]Energy, Environment Water Research Centre, The Cyprus Institute, Nicosia, Cyprus

12 [†]Now at ADDAIR, Buc, France

14 * Corresponding authors: yjanzhang@gmail.com and olivier.favez@ineris.fr

17 **Abstract**

18 Organic aerosol (OA) particles are recognized as key factors influencing air quality and climate

19 change. However, highly-time resolved long-term characterizations of their composition and

20 sources in ambient air are still very limited due to challenging continuous observations. Here,

21 we present an analysis of long-term variability of submicron OA using the combination of

22 aerosol chemical speciation monitor (ACSM) and multi-wavelength aethalometer from

23 November 2011 to March 2018 at a peri-urban background site of the Paris region (France).

24 Source apportionment of OA was achieved via partially constrained positive matrix

25 factorization (PMF) using the multilinear engine (ME-2). Two primary OA (POA) and two

26 oxygenated OA (OOA) factors were identified and quantified over the entire studied period.

27 POA factors were designated as hydrocarbon-like OA (HOA) and biomass burning OA (BBOA).

28 The latter factor presented a significant seasonality with higher concentrations in winter with

29 significant monthly contributions to OA (18-33%) due to enhanced residential wood burning

30 emissions. HOA mainly originated from traffic emissions but was also influenced by biomass

31 burning in cold periods. OOA factors were distinguished between their less- and more-

32 oxidized fractions (LO-OOA and MO-OOA, respectively). These factors presented distinct

33 seasonal patterns, associated with different atmospheric formation pathways. A pronounced

34 increase of LO-OOA concentrations and contributions (50-66%) was observed in summer,

35 which may be mainly explained by secondary OA (SOA) formation processes involving biogenic

36 gaseous precursors. Conversely, high concentrations and OA contributions (32-62%) of MO-

37 OOA during winter and spring seasons were partly associated with anthropogenic emissions

38 and/or long-range transport from northeastern Europe. The contribution of the different OA

39 factors as a function of OA mass loading highlighted the dominant roles of POA during

40 pollution episodes in fall and winter, and of SOA for highest springtime and summertime OA

41 concentrations. Finally, long-term trend analyses indicated a decreasing feature (of about -

42 175 ng m^{-3} yr^{-1}) for MO-OOA, very limited or insignificant decreasing trends for primary

43 anthropogenic carbonaceous aerosols (BBOA and HOA, along with the fossil fuel and biomass

44 burning black carbon components), and no statistically significant trend for LO-OOA over the

45 6^{+}-year investigated period.

1 Introduction

Organic aerosol (OA) particles account for a large mass fraction of submicron particulate matter (PM_1) in the atmosphere (Zhang et al., 2007) and play a key role in regional air pollution and climate (Boucher et al., 2013). Primary OA (POA) originates from direct emissions of primary sources (e.g., fossil-fuel and biomass combustion). Secondary OA (SOA) is formed from atmospheric oxidation processes of gas precursors, i.e., volatile organic compounds (VOCs) (Kroll and Seinfeld, 2008; Hallquist et al., 2009; Nozière et al., 2015). Some typical SOA formation processes in the atmosphere, such as photochemistry (Xu et al., 2017), aqueous-phase oxidation (Gilardoni et al., 2016), and heterogeneous reaction (Xu et al., 2015), are observed. Due to their multiplicity and complexity, these various sources and physicochemical mechanisms remain poorly documented and understood.

Although numerous time-limited field campaigns allowed to greatly improve our knowledge of OA properties in the last decade (e.g., Jimenez et al., 2009; Lanz et al., 2010; Zhang et al., 2011; Shrivastava et al., 2017; Li et al., 2017; Srivastava et al., 2018a, and references therein), similar studies performed on a long-term scale remain scarce and particularly challenging (Fröhlich et al., 2015a; Schlag et al., 2016; Bozzetti et al., 2017; Daellenbach et al., 2017; Sun et al., 2018). Long-term observations with high temporal resolution and source apportionment of OA are nevertheless necessary to better quantify the contribution of airborne OA particles to air quality and to set-up scientifically-sound emission control strategies. They can also contribute to a better understanding of the atmospheric fate of OA and reduce uncertainties associated with its (in)direct radiative forcing.

Online aerosol characterization techniques, such as aerosol mass spectrometry (AMS), have demonstrated their capacity to improve our knowledge of key aerosol chemical components − such as OA - by providing highly time-resolved mass spectral data for the nonrefractory PM_1 fraction (NR-PM_1) (Jayne et al., 2000; Canagaratna et al., 2007). Using receptor model approaches, especially positive matrix factorization (PMF) (Paatero and Tapper, 1994), OA measured by AMS techniques can be further portioned into various source factors using statistic models (Ulbrich et al., 2009; Zhang et al., 2011). For example, hydrocarbon-like OA (HOA) is frequently identified within urban environments and attributed to primary emissions from fuel consumption (Zhang et al., 2007; Jimenez et al., 2009), while

biomass burning OA (BBOA) is often resolved specifically during cold seasons or within wild fire plumes (Alfarra et al., 2007; Lanz et al., 2010; Zhou et al., 2017). Oxygenated OA (OOA), commonly considered as a surrogate for SOA, is ubiquitously observed in urban, suburban and remote environments (Zhang et al., 2007; Srivastava et al., 2018a; Zhang et al., 2011; Crippa et al., 2014). OOA can be further separated into different fractions, being for instance classified according to its atmospheric ageing described as more oxidized (MO-OOA) or less oxidized (LO-OOA) compared to each other (Jimenez et al., 2009; Ng et al., 2011a; Sun et al., 2018). Different OOA factors can also be identified as relevant to various sources of SOA precursors, such as anthropogenic activities (e.g., traffic and biomass burning emissions) (Gilardoni et al., 2016; Gentner et al., 2017) and biogenic emissions (e.g., isoprene and monoterpenes) (Xu et al., 2015; Zhang et al., 2018; Freney et al., 2018) in specific regions and/or seasons. Such source apportionment has the potential to assess the efficiency of air pollution mitigation by current emission control strategies.

Based on being better suited for long-term monitoring applications due to lower cost and easier maintenance than AMS, an aerosol chemical speciation monitor (ACSM) has been designed to provide continuous measurements of the main non-refractory chemical species within submicron aerosols (Ng et al., 2011b). As for the AMS, OA mass spectra obtained by the ACSM can be used in PMF analysis for quantification of OA sources (e.g., Sun et al., 2012; Fröhlich et al., 2015b; Zhang et al., 2015). So far, several time-extended OA source apportionment studies have been reported based on ACSM measurements at various sites (Canonaco et al., 2015; Fröhlich et al., 2015a; Schlag et al., 2016; Reyes-Villegas et al., 2016; Rattanavaraha et al., 2017; Sun et al., 2018). However, these studies have been limited to periods up to 2-year durations.

The longest ACSM timeseries recorded so far (from end of 2011 onwards) is used here to investigate OA sources at a regional background site of the Paris region (France), which is one of the largest urbanized regions in Europe. It has already been demonstrated that OA plays a dominant role in controlling atmospheric pollution in this region (Bressi et al., 2013; Petit et al., 2015). Furthermore, time-limited (typically, 1–2 months) measurement campaigns demonstrated that primary fine aerosols are mainly influenced there by traffic emissions all over the year and residential wood burning during cold seasons, while secondary aerosols originate from both local production and regional transports (Sciare et al., 2011; Crippa et al.,

108   2013a, Crippa et al., 2013b, Petit et al., 2014; Srivastava et al., 2018b). Furthermore, such a

109   background site can be considered as representative of air quality at a regional scale, including

110   neighboring northwestern countries (Bressi et al., 2013; Bressi et al., 2014). In the present

111   study, main OA factors were identified and quantified from seasonal PMF analyses (total 25

112   seasons) on the 6[+]-year ACSM datasets, with the objective of understanding sources and long-

113   term temporal trends of these factors. In this respect, sporadic and/or minor OA sources were

114   not accounted in this study. The seasonal variations, weekly and diel cycles, as well as the

115   long-term temporal trends of the major OA factors were investigated. The relative

116   contributions of the various POA and SOA fractions were also plotted as a function of total

117   submicron OA loadings with the objective to better identify the main OA sources responsible

118   for regional pollution episodes. Finally, the geographical origins of high loadings of SOA factors

119   were investigated using air mass back-trajectory analyses.

120

2 Sampling site and instrumentation

Long-term submicron aerosol on-line measurements used in this study were performed from 1st of November 2011 to 26th of March 2018 at the SIRTA facility (Site Instrumental de Recherche par Télédétection Atmosphérique, 2.15 °E, 48.71 °N; http://sirta.ipsl.fr/). This exploratory platform is part of the European Aerosols, Clouds, Trace gases Research InfraStructure (ACTRIS, www.actris.eu) (e.g., Pandolfi et al., 2018). It is located 25 km southwest of Paris city center and is considered as representative of the background air quality of the Paris region (Haeffelin et al., 2005; Petit et al., 2015). More information about the environmental condition features of the sampling site area has been given in the introduction (paragraph 5) above.

Major submicron aerosol chemical species i.e., OA, nitrate, sulfate, ammonium, and chloride, were measured using a quadrupole ACSM. These measurements were performed continuously, always using the same instrument. Over the whole investigated period, the data capture was of about 87%, and missing data is corresponding to two field campaigns performed elsewhere (in fall 2012 and March 2013) and to few technical breakdown and maintenance periods. Briefly, fine aerosols are sampled into the ACSM system through a 100 μm diameter critical orifice mounted at the inlet of the PM$_1$ aerodynamic lens (Liu et al., 2007; Ng et al., 2011b). Then, submicron aerosol particles are impacted and vaporized at the temperature (*T*) of about 600 °C and detected using electron impact (70 eV) ionization mass spectrometry. The ACSM was operated at a time resolution of about 30 min with a scan rate of 0.2 s amu^{-1} from *m/z* 12 to 150 amu (atomic mass unit). Coarse particles were removed upstream using an URG cyclone separator (with the size cut-off diameter of 2.5 μm). Calibrations of the detector response factor were performed regularly (typically every 6 months) using ammonium nitrate solutions (Ng et al., 2011b; Freney et al., 2019). The 1.4 default value was used for the OA relative ion efficiency for the whole dataset (Canagaratna et al., 2007). The composition-dependent collection efficiency correction recommended by Middlebrook et al. (2012) has been applied to the whole ACSM data used here. The accuracy of these ACSM measurements and the overall good working conditions of the instrument were verified through the participation to the ACTRIS ACSM intercomparison exercises that took place at SIRTA in November - December 2013 (Crenn et al., 2015; Fröhlich et al., 2015b) and March - April 2016 (Freney et al., 2019 and Figure S1).

152   Co-located multi-wavelength aethalometer (Magee Scientific) datasets were also
153   available for the purpose of the study, providing complementary information on equivalent
154   black carbon (eBC) concentrations and sources. Two aethalometers were used successively:
155   from November 2011 to February 2013 (AE31 model) and then from March 2013 to March
156   2018 (AE33 model). Both instruments measure aerosol light attenuation at seven wavelengths,
157   i.e., 370, 470, 520, 590, 660, 880 and 950 nm. The detailed descriptions of the AE31 operation
158   at SIRTA and aethalometer data analysis can be found in Petit et al. (2015). The AE33 is an
159   advanced aethalometer version, which allows better assessment and compensation of the
160   filter-loading effect using two simultaneous light attenuation measurements performed at
161   different rates of particle accumulation onto the filter tape (Drinovec et al., 2015; Drinovec et
162   al., 2017). An excellent agreement (R=0.94, slope=1.006$\pm$0.006) between AE31 and AE33 for
163   measuring eBC mass concentrations has been demonstrated by Drinovec et al. (2015),
164   suggesting negligible influence of measurement uncertainties between the two mode
165   instruments on quantification of eBC concentrations. In this work, the mass concentration of
166   eBC was estimated from attenuation measurement performed at 880 nm as described by Petit
167   et al. (2015) and Zhang et al. (2018). A correction factor of 1.64 was applied to raw absorption
168   data delivered by the instrument as recommended within the ACTRIS network (Zanatta et al.,
169   2016). Furthermore, eBC could be discriminated between its two main combustion sources,
170   i.e., fossil-fuel combustion (eBC$_{ff}$) and wood burning emissions (eBC$_{wb}$) using the aethalometer
171   model (Sandradewi et al., 2008; Favez et al., 2010; Sciare et al., 2011; Drinovec et al., 2015).
172   For these calculations, absorption Angström exponent (AAE) values - in the wavelength range
173   470-950 nm - of 0.9 and 1.7 for eBC$_{ff}$ and eBC$_{wb}$, respectively, were estimated by the AAE
174   distributions observed in this study (see Figure S2). Meanwhile, those values are in a good
175   agreement with the recommended values by Zotter et al. (2017).

176   In addition to ACSM and AE33 measurements, co-located off-line analyses were
177   performed from daily (24 h) PM$_{2.5}$ filter samples, collected and analyzed for their content in
178   elemental and organic carbon (OC and EC, respectively) following the ACTRIS
179   recommendations (Zanatta et al., 2017; Zhang et al., 2018). Briefly, filters were collected using
180   a low volume sampler (Partisol Model 2025; Thermo Scientific) equipped upstream with a VOC
181   denuder system. Mass concentrations of OC and EC from August 2012 to March 2018 were
182   then quantified using a Sunset Lab OC/EC analyzer implemented with the EUSAAR-2 thermal-

optical protocol (Cavalli et al., 2010). As shown in Figure S3, good agreements are obtained between eBC and EC measurements (r^2 = 0.79, slope = 0.94; N=1185 as well as between OA and OC measurements (r^2 = 0.68). The slope of 2.14 obtained between submicron OA measured by the ACSM and PM$_{2.5}$ OC filter-based measurements corresponded to the higher range of values generally observed at (sub)urban background sites - typically 1.6-2.2 (e.g., Bae et al., 2006; Aiken et al., 2008; Favez et al., 2010; Sun et al., 2011; Canagaratna et al., 2015 and references therein) - and may be partly explained by the fact that the filter sampling set-up has been designed to minimize positive sampling artefacts but do not prevent from negative ones. Results obtained from these comparisons with filter-based measurements supported the validity of the datasets used in the present study.

Co-located measurements of nitric oxide (NO) and nitrogen dioxide (NO$_2$) were performed with a NO$_2$/NO/NOx analyzer (model T200UP, Teledyne API, USA). Data measurements were used for further constrain traffic related OA sources. The meteorological parameters, including T, relative humidity (RH), wind speed (WS), wind direction (WD), boundary layer height (BLH), and precipitation were obtained from the main SIRTA ground-based meteorological station, (located at about 4 km North-East of the aerosol monitoring site). It should be noted that the BLH data was achieved in combining a diagnostic of the surface stability from high-frequency sonic anemometer measurements and light detection and ranging (LIDAR) attenuated backscatter gradients from aerosols and clouds (Pettie et al., 2015; Dupont et al., 2016).

3. Data treatment procedures

3.1 PMF analysis

The OA source apportionment was performed using PMF algorithm (Paatero and Tapper, 1994). Organic concentration and error matrices were exported from the ACSM Local software (v 1.5.11.2). Only m/z ranging from 13 to 100 was applied in the PMF analysis due to larger uncertainties for larger m/z ions and large interferences of naphthalene (m/z 128) signals (Sun et al., 2012). Downweighting of the m/z 44-group ions for the PMF model analysis was performed following procedures implemented in the ACSM Local software and following data treatment strategy proposed by Ulbrich et al. (2009).

When using PMF, it may be difficult to distinguish between factors with similar spectral profiles, especially for ACSM datasets, which are associated with larger uncertainties compared to AMS (Sun et al., 2012; Zhang et al., 2015; Fröhlich et al., 2015b). The source finder (SoFi) toolkit, implemented with the ME-2 solver (Paatero, 1999), has been developed by Canonaco et al. (2013) to better address this limitation. SoFi provides robust functions which allow to constrain chosen factor profiles and/or timeseries. In particular, the a-value approach makes use of range-defining scalar values (with a values ranging from 0 to 1) in order to better elucidate specific PMF factor(s) profile(s) with a chosen degree of freedom; the highest the a value and the less constrained the OA profile (Canonaco et al., 2013). In the present work, this a-value approach has been used to constrain profiles of POA factors. Some previous studies have already been performed at SIRTA using high resolution time-of-flight AMS (HR-ToF-AMS) along with PMF analysis during short-time campaigns (typically around 3-4 weeks), leading to the identification of HOA, BBOA, as well as a cooking OA (COA) factor (Crippa et al., 2013a; Crippa et al., 2013b; Fröhlich et al., 2015b). Mass spectra obtained from these studies were used here as references to constrain POA factors, because of the prior know source information as constraints. Conversely, mass spectral profiles of possible OOA factors were left unconstrained. It should be noted that Crippa et al. (2013a) resolved up to 3 different type of OOA factors and/or a marine OA (MOA) factor when combining HR-ToF-AMS and proton-transfer-reaction mass spectrometer (PTR-MS) datasets obtained during a summer and a winter campaign at SIRTA.

OOA factor profiles may differ with time, notably due to seasonal variations of several parameters such as meteorological conditions, photochemistry, atmospheric lifetime, air masses origin, and/or of gaseous precursor origins. In order to better account for such variability, individual PMF analyses were performed on a 3-month basis, i.e., winter (December-January-February), spring (March-April-May), summer (June-July-August), and fall (September-October-November), with a total number of 25 different PMF runs (7 for winters and 6 for each of the other seasons). November 2011 and March 2018 data were included in the winter 2011-2012 and winter 2017-2018 analyses, respectively.

To evaluate the influence of the chosen temporal PMF window (i.e., time duration of data used in ME-2 runs) on the seasonal ME-2 model results, different timeframes (i.e., 15, 30, 60, 90 and 120 days) were tested. As shown in Figure S4 (with 2017 winter data as an example),

244 the excellent consistency of those results from different scenarios suggest very limited

245 influence of the given PMF windows on determining the outputs of ME-2 analyses. To better

246 assess the variations in primary and secondary OA in different seasons over the 6⁺-year period

247 and to allow for some degrees of freedom within the model runs, the main OA factors,

248 including both POA factors (HOA and BBOA) and two SOA factors (a less oxidized OOA (LO-

249 OOA) and a more oxidized OOA (MO-OOA)), were calculated as the average of 50 convergent

250 ME-2 runs with the *a* values varying from 0 to 0.4. Moreover, results obtained with an *a*-value

251 of 0.2 were also compared to these results for sensitivity analyses (Figure S5). The diagnostics

252 of the final OA-factor solution are further discussed in section 4.1.

253

3.2 Influence of biogenic SOA

255 Biogenic SOA (BSOA) might have a significant influence on OA loadings in mid-latitude regions

256 during summertime and be further apportioned using AMS techniques (e.g., Leaitch et al.,

257 2011; Canonaco et al., 2015). For that reason, influence of this biogenic OA source was

258 specifically investigated in the present study. To do so, BSOA derived from terpene emissions

259 (BSOA$_t$) was taken as a surrogate for total BSOA and the *T* dependence of the BSOA$_t$ formation

260 process yield during summertime was simulated using a terpene emission model (Goldstein

261 et al., 2009; Schurgers et al., 2009; Leaitch et al., 2011 and references therein). This model is

262 designed to quantify biogenic emissions over global and regional scales. The emission rate (γ)

263 is estimated by an exponential curve function (Eq. 1), which is describing the relation between

264 terpene γ and leaf *T*. As we assumed changes in leaf *T* as same as ambient *T*, which could then

265 result in part of uncertainties for the model calculation. In addition, this *T*-dependent model

266 reflects vapour pressure changes caused by *T*, however, changes in vapour pressure due to

267 changes in the concentrations in the storage pool of terpene are not covered by the model

268 (Schurgers et al., 2009). Therefore, this emission model is useful to simulate the short-term

269 emissions because of *T* changes (Schurgers et al., 2009).

270 $$\gamma = \gamma_0 \times e^{\beta(T-303)} \quad (1)$$

271 where γ_0 stands for the emission rate (μg g^{-1} h^{-1}) at standard conditions, and β is an empirical

272 constant chosen here to be equal to 0.09 K^{-1} (Schurgers et al., 2009; Leaitch et al., 2011). As

273 reported by previous studies, biogenic terpene emissions could be a major source of such PMF

274 LO-OOA factor observed during summertime in western Europe (e.g., Canonaco et al., 2015;

275 Daellenbach et al., 2017; Daellenbach et al., 2019). Given that, $BSOA_t$ was assumed to be

276 mainly included in the LO-OOA fraction in the present work, and $BSOA_t$ estimated

277 concentrations were compared to LO-OOA concentrations data points corresponding to the

278 daytime maximum T (at approximately 16:00 – 17:00 local time) in summer. Assuming that

279 LO-OOA could actually be mostly composed of $BSOA_t$ during this period of the day and

280 following the procedure described by Leaitch et al. (2011), the daily mass concentrations of

281 $BSOA_t$ were estimated as follows:

$$BSOA_{t,estimated} = LO - OOA_{(Observed\ at\ Tmin)} \times \frac{\gamma}{\gamma_{(Tmin)}} \qquad (2)$$

283 where T_{min} corresponds to the lowest daily maximum T observed across the investigated

284 summer seasons (i.e., 12°C ± 1°C) and $LO-OOA_{(observed\ at\ Tmin)}$ corresponds to the mean LO-OOA

285 concentration obtained for these data points (0.7 ± 0.3 µg m^{-3}, N = 17).

286

3.3 Trend analysis

288 The multi-year trends of monthly mean OA factors and total OA, as well as other chemical

289 components (including eBC_{wb}, eBC_{ff}, nitrate, sulfate and total PM_1) were analyzed using the

290 Mann-Kendall (MK) trend test (Mann, 1945). The trend slope was calculated using Theil-Sen

291 estimator (Sen, 1968). Before performing MK trend test, the normality and seasonality of the

292 OA factors were examined, respectively. The normality of the mass concentrations of the OA

293 factors was examined by the Shapiro-Wilk normality test (Shapiro and Wilk, 1965). As a result

294 of the Shapiro-Wilk normality test, all datasets of the mass concentrations of the four OA

295 factors were not normally distributed cases. The MK test associated with Sen's estimator of

296 slope is insensitive to outliers, while it is not appropriate for the chosen dataset with

297 significant seasonality. The Kruskal-Wallis test (Kruskal and Wallis, 1952) was performed to

298 evaluate the seasonality of monthly average datasets at the 5% significance level. If the

299 seasonality of the data is insignificant, the MK test was used for the trend analysis, while the

300 seasonal MK test was then applied for the data with significant seasonality. In addition, to

301 further compare the differences between the MK test and the seasonal MK test in our trend

302 analysis, both methods have been applied for all data sets (see Table S1). The trend

303 computation was performed here using a R trend package (Pohlert, 2018).

304

3.4 Air mass back-trajectory analysis

306 The HYbrid Single Particle Lagrangian Integrated Trajectory model (Hysplit) Draxler and Rolph,

307 2003; Stein et al., 2015) was applied to calculate 72-h back trajectories hourly arriving at SIRTA

308 at a height of 100 m above ground level, based on GDAS meteorological data. The potential

309 source contribution function model (PSCF) (Polissar et al., 1999) was used in this study to

310 investigate the potential source origins that may contribute to high concentrations of OA

311 factors at SIRTA. This analysis was achieved with a resolution of 0.2° × 0.2° for each grid cell,

312 using the ZeFir toolkit (Petit et al., 2017). The probability function for a given grid cell (i, j),

313 where i stands for the latitude and j for the longitude, is related to observed concentrations

314 that are higher than a threshold value, which is defined by Eq. (3):

$$315 \qquad PSCF_{(i,j)} = \left(\frac{m_{ij}}{n_{ij}} \right) \cdot w_{ij} \qquad (3)$$

316 where m_{ij} is the total number of selected trajectory endpoints (i, j) associated with receptor

317 concentrations of PMF factors higher than the threshold value, and n_{ij} is the total number of

318 back trajectory endpoints at each grid cell (i, j). The 75th percentile of each OA factors during

319 the entire study was used as the threshold value to calculate m_{ij}. To reduce uncertainty caused

320 by small n_{ij} values for the PSCF modelling, an arbitrary weighting function (w_{ij}) was applied

321 (Waked et al., 2014). To minimize the influence of some trajectories on the possible pathways

322 of air mass transport, observed data points associated with low wind speed conditions (WS <

323 4 m s^{-1}) were filtered out. In addition, observed data points at SIRTA during the period with

324 any hourly precipitation events (precipitation > 0 mm) were removed to reduce influence of

325 wet deposition on ambient aerosol concentrations.

326

4 Results and discussion

4.1 Identification of the main OA factors

4.1.1 Determination of the optimum factor number

The optimal number of PMF OA factors shall be determined by the distribution of the main sources at a given sampling site. Based on results obtained from the compilation of previous AMS studies reported in the Paris region, two POA factors - HOA and BBOA - and two OOA fractions - MO-OOA and LO-OOA – are undoubtedly major fraction of submicron aerosols in Paris area over the year (Crippa et al., 2013a; Crippa et al., 2013b; Freutel et al., 2013; Petit et al., 2014; Fröhlich et al., 2015b). Another POA source, i.e., COA, has also been identified using HR-ToF-AMS during previous campaigns in Paris region (Crippa et al., 2013a; Crippa et al., 2013b; Fröhlich et al., 2015b). However, the distinction between COA and HOA factors based solely on ACSM measurements remains challenging due to highly similar mass spectra and uncertainties associated with the ACSM low mass spectral resolution (Petit et al., 2014; Fröhlich et al., 2015b).

To better assess a potential role of COA in our source apportionment study, several ME-2 runs were conducted constraining either three POA factors (HOA, BBOA, COA) or two (HOA, BBOA). In these tests, POA reference mass spectra determined by Fröhlich et al. (2015b) were employed as anchor profiles (with a-values ranging from 0 to 0.4 with steps of 0.05). PMF solutions with a factor number ranging from 3 to 6 were investigated on ACSM datasets corresponding to different seasons of different years (December 2011 - February 2012, March - May 2015, June - August 2017, September - November. 2017, December 2017 - February 2018). Results obtained from these preliminary individual PMF runs showed very good consistency between them with two unconstrained OOA factors - MO-OOA and LO-OOA - always appearing in the 4-factor (with constrained HOA and BBOA factor) and 5-factor (with constrained HOA, BBOA and COA factor) solutions. Conversely, 3- and 6-factor PMF analyses generally led to unsatisfactory solutions.

Figures 1 and S6 present results obtained for the 4- and 5-factor solutions, respectively, for the winter 2017-2018 period, taken here as an example. In both cases, mass spectra are in good agreement with those reported in the literature. However, the COA and BBOA factors are displaying very similar diel patterns, leading to surprisingly good correlations between the two factors (Figure S7). In order to further evaluate possible COA contribution at SIRTA, we applied a m/z-tracer algorithm (Mohr et al., 2012) trying to identify pure cooking aerosol signals. The distribution of the estimated COA signals is centered at about 0, as illustrated by

360 Figure S8. This could be probably explained by very little pure cooking influence that could not

361 be quantified by the lower resolution quadrupole ACSM than AMS, which is logically in

362 agreement with negligible cooking source at the sampling site area nearby. Altogether, it could

363 then be concluded that the constrained COA-like aerosols at SIRTA were primarily linked with

364 wood burning emissions, while pure cooking aerosols were probably present in too low

365 loadings to be properly quantified within the present study. This assumption is consistent with

366 conclusions drawn by other studies performed at SIRTA, e.g., based on an online (ACSM)

367 dataset (Petit et al., 2014) and a combining PMF method using online (ACSM) and offline (4-h

368 filter sampling) datasets (Srivastava et al., 2019), as well as other studies showing that the COA

369 factor could not be solely attributed to cooking aerosols (e.g., Freutel et al., 2013, Dall'Osto et

370 al., 2015).

371 Therefore, the 4-factor solution, including two constrained POA factors (BBOA and

372 HOA) and two unconstrained factors, was chosen here as the ''best estimate'' for the PMF

373 runs performed over the long-term dataset. A total of 25 seasonal and individual PMF analyses

374 were then conducted using a similar procedure. The seasonal OOA factor mass spectra are

375 presented in Figure S9, showing high seasonal consistency for each OA factor. Moreover, as

376 shown in Figure S10, the distribution of residuals derived from the these 4-factor solution ME-

377 2 runs was sharply centered at around 0, suggesting insignificance of possible unresolved OA

378 factor(s). The correlations of OA factors with their tracers were examined to globally evaluate

379 the 4-factor PMF solution (see Figures S11 and S12). As shown in Figure S11a, HOA is

380 correlated well (r^2=0.54) with NOx, a common tracer of primary combustion sources (e.g.,

381 traffic emissions). While HOA shows a relatively weaker correlation (r^2=0.33) with eBC$_{ff}$ (Figure

382 S11b), this could be explained by two possible reasons, i) uncertainties of Aethalometer model

383 which however could not be evaluated by the present study, and ii) the HOA factor here could

384 not be reprehensive for pure fossil-fuel combustion POA. BBOA presents an overall good

385 correlation (r^2=0.50) with eBC$_{wb}$ (Figure S11c), suggesting important influence of wood

386 burning emissions on this factor production. Based on the filter-based dataset, primary OC

387 (POC) and secondary OC (SOC) were calculated using a method of OC-to-EC mass ratio (see

388 Figure S12). Overall, POA (sum of HOA and BBOA) versus POC (r^2=0.47) and SOA (sum of LO-

389 OOA and MO-OOA) versus SOC (r^2=0.38) have acceptable correlations during the entire filter

390 measurement period. Thus, all of these comparison results could additionally support our

391 "best estimation" for selecting such 4-factor PMF solution across the entire period.

392

393 **4.1.2 Source attribution**

394 BBOA mass spectra are quite constant throughout the seasons, and present

395 characteristic peaks at *m/z* 29, 60, and 73 indicative of biomass burning combustion (Figure

396 S9). As shown in Figure 2a, BBOA diel cycles displayed well-marked patterns with strong

397 nighttime maxima. This confirms the predominance of residential wood burning activities on

398 BBOA concentrations at SIRTA and in the Paris region, as already shown previously (e.g., Favez

399 et al., 2009; Sciare et al., 2011; Crippa et al., 2013b; Petit et al., 2014). As expected, BBOA diel

400 cycles are similar to the ones obtained for eBC_{wb}, except for small eBC_{wb} morning peaks that

401 were not observed for BBOA (possibly due to uncertainties of the aethalometer model).

402 Interestingly, the higher concentrations of eBC_{wb} and BBOA were observed on Saturday and

403 Sunday, reflecting the week-end effect likely due to enhanced residential wood burning

404 emissions.

405 Compared to BBOA, HOA shows a more complex weekly diel pattern (Figure 2b). Its

406 pattern is generally similar to eBC_{ff} and NO_x (both being considered here as markers for traffic

407 emissions). HOA presents two peaks during working day, one in the morning and another in

408 the evening. Morning peaks, occurring during traffic rush hours are clearly indicative of road

409 transport contributions, confirming HOA as a proxy for traffic emissions. However, HOA

410 evening peaks occurs globally later than eBC_{ff} and NO_x ones (9:00-10:00 PM vs. 7:00 PM,

411 respectively) and much lower ratios are observed between HOA and eBC_{ff} in the morning than

412 in the evening. This might be partly explained by i) higher eBC traffic emission factor in the

413 morning and/or ii) impacts of residential heating sources, e.g., wood and/or heating oil

414 burning (Lin et al., 2018), on the HOA concentrations in the late evening. Moreover, eBC_{ff}

415 shows a clear weekend effect, with less-pronounced pattern on Saturday and Sunday due to

416 road transport reduction, while HOA displays intense nighttime peaks during weekend. This

417 HOA mean pattern was substantially influenced by winter data, whereas summertime

418 patterns display better consistency between HOA, eBC_{ff} and NO_x (Figure S13). Altogether,

419 these results suggest that this HOA is considered as a mixed factor partly composed of both,

420 traffic and residential heating aerosols. This statement is in good agreement with conclusions

421 from complementary studies showing wood burning contribution to HOA at the same site

422 (Petit et al., 2014; Srivastava et al., 2019).

423   As presented in Figures 1a and S9, MO-OOA mass spectra present a strong peak at m/z

424 44. In fact, this spectrum has been widely reported as low volatility OOA (LV-OOA) and

425 considered as composed of highly oxidized and aged SOA (Lanz et al., 2007; Ulbrich et al., 2009;

426 Zhang et al., 2011; Ng et al., 2011a). Overall, MO-OOA had a weak correlation (r^2=0.23) with

427 sulfate during the entire period, supporting their different source origins to some extent.

428 Compared to the poorly pronounced diel variability of sulfate, this MO-OOA factor exhibits a

429 slight enhancement at nighttime (Figure 2c), suggesting a possible local formation mechanism

430 involving nighttime chemistry, on top of its overall regional feature. The geographic origins of

431 the MO-OOA factor are further discussed in section 4.2.1 for each season.

432   The mass spectra of LO-OOA in this study present a higher m/z 43 and a lower m/z 44

433 (Figures 1a and S9), compared to MO-OOA, which is consistent with the mass spectral pattern

434 of previously reported freshly-formed semi-volatile OOA (SV-OOA) (Jimenez et al., 2009; Ng

435 et al., 2010). The diel variations of LO-OOA display higher concentrations during nighttime

436 than daytime (Figure 2d), with relative variations much more pronounced than for the MO-

437 OOA diel pattern, highlighting important roles of nighttime chemistry and/or gas-particle

438 partitioning in the LO-OOA formation. These results support different formation pathways of

439 the two OOA fractions. In addition, LO-OOA and nitrate present different diel cycles,

440 suggestive of different formation processes and sources between each other. Different diel

441 cycles of LO-OOA in different seasons have been also observed, which are further discussed

442 in section 4.2.1. In winter, LO-OOA mass spectra has higher contributions of m/z 29 as well as

443 elevated m/z, i.e., starting from m/z 60, than during other seasons (Figure S9). Such

444 characteristics suggest a major influence of biomass burning emissions onto the LO-OOA

445 factor during wintertime, as previously proposed from measurements in the Paris region (e.g.,

446 Crippa et al., 2013b). Conversely, in summer, this factor may be significantly influenced by

447 BSOA formation (Canonaco et al., 2015; Daellenbach et al., 2017). To investigate this possible

448 origin, we checked if the summertime LO-OOA concentrations at higher daily T were following

449 T dependence similar to the one expected for the formation of terpene SOA, as explained in

450 section 3.2. Results of these calculations are presented in Figure 3. The LO-OOA

451 concentrations substantially increase with T, showing a good agreement with the estimated

452 $BSOA_t$ formation exponential profiles. However, when comparing with estimation derived

453 from Eq. (2) (referred to Figure 3), the observed LO-OOA displays substantially higher loadings

454 than estimated $BSOA_t$ at highest concentration range. This could be partly due to the influence

455 of regional transports and atmospheric dilution on aerosol loadings and some possible

456 uncertainties (such as unclear formation mechanism of biogenic SOA at SIRTA), which were

457 not considered in the $BSOA_t$ estimation. These comparison results between observation and

458 estimation indicates that the LO-OOA factor observed in summer might be mainly associated

459 with biogenic sources. This is aligned with the VOCs seasonal patterns observed in the Paris

460 region (Baudic et al., 2016), although the underlying SOA formation mechanism is still unclear

461 and needs to be further investigated (Beekmann et al. 2015). Further discussion about

462 seasonality of the LO-OOA factor is given in section 4.2.1.

463

464 **4.2 OA factor temporal variations**

465 Figure 4 presents timeseries of total submicron OA and its four main factor components

466 (namely HOA, BBOA, MO-OOA and LO-OOA) together with key meteorological parameters:

467 BLH, RH and T, during the entire investigated period. Most meteorological parameters present

468 seasonal cycles. Total submicron OA presented dynamic variations during all seasons with

469 hourly average concentrations ranging from 0.03 to 77.5 µg m^{-3} and daily average values from

470 0.2 to 41.3 µg m^{-3}. There was no clear seasonality for the total monthly average OA

471 concentrations, varying from 4.8 to 5.1 µg m^{-3}. However, each individual OA factors displayed

472 intra and inter-annual variations, which are discussed in this section.

473

474 **4.2.1. Monthly and seasonal variations of OA factors**

475 Figure 5 illustrates monthly average concentrations obtained for each OA factor over the

476 studied period. HOA monthly concentrations vary from 0.4 to 1.3 µg m^{-3} and display a

477 statistically insignificant seasonal trend ($p > 0.05$, Figure 5a). Nevertheless, the mass

478 concentration of HOA is nearly twice higher during cold months (in the range of $0.9 - 1.3$ µg

479 m^{-3}, from November to March) than in other months (in the range of $0.4 - 0.5$ µg m^{-3} from

480 April to October). This monthly cycle of HOA could be partially explained by lower BLH

conditions and influence of more intense emissions of biomass burning in cold seasons than in warm seasons (Figures 4 and S14). As illustrated by Figure S15, HOA clearly presents two peaks (in the morning and late evening) for each season. The evening HOA peak is about 1.3-1.5 times higher than the morning peak in winter and fall seasons when high loadings of BBOA are observed as well. Although dynamic processes (establishment of a stable nighttime boundary layer) cannot be excluded, these results point to a possible contribution of biomass burning emissions to the HOA factor in the evening during cold months, as discussed before from the diel cycles of OA factors.

As shown in Figure 5b, BBOA displays a statistically significant seasonal pattern trend ($p < 0.0001$) with higher monthly mean concentrations ($1.1 - 1.9$ µg m^{-3}) during cold months (November – March) than during the April – September period ($0.3 - 0.5$ µg m^{-3}). This seasonal dependence of wood burning emissions is associated with the residential heating activities in the Paris region. BBOA presents a seasonal dependence of its diel cycle, as presented in Figure S15. In particular, BBOA shows an evident peak at evening/nighttime in winter, spring, and fall, while it presents a stable diel cycle during summertime. The highest seasonally-averaged nighttime peak (up to 2.4 µg m^{-3}) is observed in winter, highlighting a significant enhancement of wood burning emissions and influence of meteorological conditions (such as low BLH) during this season (Figure S14).

Monthly average mass concentrations of MO-OOA present a significant seasonal trend ($p < 0.05$), varying from 1.0 in September to 3.5 µg m^{-3} in March (Figure 5c), in agreement with previous studies performed in Europe (Schlag et al., 2016; Daellenbach et al., 2017; Bozzetti et al., 2017). The highest MO-OOA mass concentrations observed in the cold months are somehow similar to the seasonal variation of BBOA. MO-OOA diel cycles also present a seasonal variation, with significant increase during evening/nighttime in winter, spring, and fall (Figure S15). In order to minimize the effect of atmospheric dilution and regional transport, the mass concentration of MO-OOA was normalized to sulfate, the latter one being considered as a regional secondary production marker (Petit et al., 2015 and Figure S16). As shown in Figure S16, the correlations between MO-OOA and sulfate are found to be strongly BBOA- and wind speed-dependent. For high wind speed and low BBOA concentrations, the mean MO-OOA-to-sulfate ratio is close to 1, while it reaches up to 8 under high BBOA and low-to-medium wind speed. This is consistent with the assumption of an enhancement of MO-OOA formation

in the presence of substantial biomass burning emissions, which have been reported as a major anthropogenic SOA source (Heringa et al., 2011; Tiitta et al., 2016; Bertrand et al., 2017; Stavroulas et al., 2019; Daellenbach et al., 2019). Actually, both MO-OOA and LO-OOA factors may be significantly influenced by wood burning emissions as they are displaying similar correlations with eBC_{wb} for highest MO-OOA-to-sulfate ratios during wintertime (Figure 6).

As shown in Figure S17, high concentrations of MO-OOA are generally observed at high RH (> 80 %) and low T (< 0 °C) conditions during wintertime. This low air temperature condition could be associated with a possible scenario for increase of the MO-OOA precursors emissions from biomass burning by residential heating activities during wintertime. As Figure S18 shows, the MO-OOA-to-sulfate ratio shows a significant enhancement as a function of RH in winter, suggesting that the aqueous-phase heterogeneous processes may represent an important pathway for the local MO-OOA formation in winter as proposed by Gilardoni et al. (2016). Conversely, there are no obvious RH-T dependent patterns for the MO-OOA in spring (Figure S17), indicative of more complex formation processes during this season. In summer, MO-OOA displays evident increase from early afternoon to evening (Figure S15), suggesting significant local photochemical production of SOA particles in summer with higher T and increased solar radiation (Petit et al., 2015). As a matter of fact, MO-OOA presents high concentrations under high T (> 25 °C) and low RH (< 65%) summertime conditions (Figure S17). In conclusion, and despite relatively constant mass spectra all over the year, MO-OOA appears to originate from various seasonal-dependent formation pathways and sources (such as biomass burning and biogenic sources), that should still be investigated in more detail.

The LO-OOA mass spectra with high f_{43} / f_{44} ratios are frequently observed in spring, summer and fall, whereas a lower ratio is obtained for winter (Figure S9). These different mass spectra of LO-OOA could be partially explained by seasonal-dependent formation mechanisms and sources. The monthly mean mass concentrations of LO-OOA vary from 0.8 to 3.6 µg m^{-3} (Figure 5d) and shows a statistically significant seasonality (p < 0.001) with higher concentrations during warm months and lower during cold months. As discussed above, the high summertime LO-OOA concentrations are assessed to be mainly linked with BSOA formation. As presented in Figure S17, T-RH dependence of the LO-OOA factor is very different according to the season. In particular, the highest wintertime LO-OOA concentrations are mainly observed at low T and high RH conditions, suggesting that gas-particle partitioning may

play an important role in LO-OOA formation during this season. As shown in Figure 6b, LO-OOA shows a good correlation (r^2=0.55) with eBC_{wb} at high MO-OOA-to-sulfate ratio conditions during wintertime, in agreement with the case of MO-OOA, which suggests that wood burning emissions could also contribute to the LO-OOA formation during winter. This is consistent with freshly-formed SOA originating from primary biomass burning emissions, as reported by previous studies (Crippa et al., 2013b; Zhang et al., 2015; Sun et al., 2018; Stavroulas et al., 2019). In summer, the LO-OOA concentrations present strong T positive dependence while RH dependence is not clear, indicating that photochemical production of LO-OOA became more important in summer than in winter. Moreover, high concentrations of the summertime LO-OOA are observed during the two distinct time periods in one day, i.e., early afternoon (around $12:00-15:00$) and nighttime (around 22:00-05:00), which is different from the diel variations in other seasons with high concentrations only during nighttime (Figure S15). These LO-OOA diel variations may reflect different formation pathways across one day in summer. Photochemical process might dominate the LO-OOA production at daytime, while nighttime chemistry and/or gas-particle partitioning might promote its formation at low T conditions at night.

4.2.2. Long-term temporal trends

Figure 7 presents the results obtained from the trend analysis of the 6^+-year monthly timeseries of the four OA factors, total OA, the two eBC components, secondary inorganic species (sulfate and nitrate) and total PM_1 (the sum of $NR-PM_1$ and eBC). The significance and magnitude of these trends were examined using the MK p-value and Sen's slope, respectively. Annual mean mass concentrations of these OA factors and aerosol chemical species have been given in Table 1.

BBOA presents a statistically significant decreasing trend ($p < 0.05$) with a Sen's slope of about -65 ng m^{-3} per year in the Paris region. On the other hand, eBC_{wb} concentration trends appear quite stable over the investigated period. Two possible reasons may explain the discrepancy trend results between BBOA and eBC_{wb}. It may be hypothesized that a limited overall improvement of wood stove performances in the Paris region could have influence BBOA emission factors more than eBC_{wb} ones (Saleh et al., 2014), but no evidence has been

found to support this assumption. Similarly, but in the opposite way, eBC_{ff} was found to have a significant decreasing trend, while HOA trend was found to be statistically insignificant (*p*-value > 0.05). However, if removing the high concentration peaks observed in December (for which an important contribution of wood burning HOA can be expected), the MK *p*-value is reduced to be 0.03, which would be indicative of a significant decreasing trend (with a related Sen's slope of -59 ng m^{-3} per year). These results would be in line with a reduction of PM$_1$ traffic emissions (-37%) over the past years (2012-2017) in France, as estimated by the French emission inventory state operator (CITEPA, 2018). However, such trends analysis should be performed on longer datasets for a much better evaluation of the pollution control strategies (both on road transport and residential heating emissions) in the Paris region.

MO-OOA shows a significant decreasing trend (*p* < 0.05) with a Sen's slope of -175 ng m^{-3} per year. Considering the overwhelming secondary origin of this factor, this significant decreasing trend may be partially explained by an overall reduction of anthropogenic VOCs emissions (-13%) in France (CITEPA, 2018) and even in a larger spatial scale, e.g., the western European region, during 2012-2017. LO-OOA presents no significant trend (with *p* > 0.05). As discussed above, higher LO-OOA loadings may be linked to BSOA formation, especially at summertime. The stability of LO-OOA concentrations over time may be linked to limited changes in biogenic VOC emissions and/or in relevant oxidant concentrations, that control the SOA burden in the atmosphere. Effect of anthropogenic-biogenic interaction mechanisms on biogenic SOA formation - e.g., involving NO_x, as reported by previous studies in urban regions (Budisulistiorini et al., 2015; Zhang et al., 2017) - could also partially explain the limited changes for the long-term trend of LO-OOA at SIRTA. Detailed LO-OOA formation processes involved here still need to be further investigated. Nevertheless, it may be assumed that reductions of anthropogenic VOC emissions only cannot be sufficient to weaken the total SOA background concentrations in the Paris area.

The trends are more significant for total OA (*p* < 0.005, about -382 ng m^{-3} yr^{-1}), as well as for nitrate (*p* of about 0.01, and approximately -145 ng m^{-3} yr^{-1}) and total PM$_1$ (*p* of about 0.002, and approximately -644 ng m^{-3} yr^{-1}), than for sulfate (with *p* value around 0.5117). In addition to SO_2 emitted from anthropogenic sources (e.g., industrial and shipping emissions) (Hoesly et al., 2018), natural sources (e.g., volcanic emissions) (Boichu et al., 2019) could also influence sulfate budget in western Europe. This suggests that regional aerosol chemistry

604   modeling simulations by using different SO_2 emission sectors may help to further explain the

605   temporal trends of sulfate. Meanwhile, it should be noted that the sulfate trend here could

606   be probably influenced by the ACSM measurement uncertainties (Crenn et al., 2015; Freney

607   et al., 2019), which however could not be fully quantified here. Overall, these decreasing

608   trends could reflect the response of the PM concentrations to the decrease in anthropogenic

609   source emissions during these last years in Europe. Reduction in NO_x (-19%) came with a

610   negligible change in NH_3 emissions (+2%) over the French region during recent years (2012-

611   2017), which may support that the decreasing trend in particulate nitrate was likely driven by

612   the NO_x emissions control in the Paris region (CITEPA, 2018). A continuous effort to reduce

613   POA emissions and SOA precursors (VOCs) may lead to the decrease to the total both OA and

614   fine PM budgets (EMEP, 2016; CITEPA, 2018).

615

616   **4.3 OA source contribution as a function of OA concentrations**

617   Figure 8 presents the contribution of the four OA sources as a function of total submicron OA

618   mass loadings or each season along with percent changes of meteorological conditions. In

619   winter and fall (Figure 8 e and h), all meteorological parameters - except limited changes in

620   RH - show negative relationships as a function of the OA mass concentrations, confirming the

621   coincidence of low T, low WS, and/or low BLH in the formation of pollution episodes (Dupont

622   et al., 2016). POA contributions gradually increase from 35 % (resp. 27 %) up to 64 % (resp.

623   70 %) as a function of OA mass concentrations in winter (resp. fall) (Figure 8 a and d). These

624   results illustrate the major role of primary sources during periods with high OA concentrations

625   during the cold seasons. In particular, BBOA contribution gradually increase from 21 % (15 %)

626   to 41 % (40 %) in winter (fall) along with OA mass loading increase.

627   In spring, OA composition is radically changed and is dominated by the two OOA

628   fractions, with almost constant average contributions (68 − 77%) regardless OA concentration

629   levels (Figure 8b), indicating the major role of SOA during this season. MO-OOA presents

630   higher contributions to OA (45-53%) than LO-OOA (15-31%), suggesting that the formation of

631   aged SOA plays a key role on the build-up of episodes with high OA concentrations during

632   springtime. As shown in Figure 8f, the percent changes in T, WS, and BLH gradually decrease

633   with increasing OA concentrations. By contrast, RH shows a positive relationship with OA mass

concentrations, with the largest RH enhancement (16%) at highest OA-loading bin (> 25 μg m^{-3}). This may suggest that high RH being the most favorable environment condition for SOA formation during springtime OA pollution episodes, as supported by a high contribution of OOA factors at the highest OA concentration level (Figure 8b). In addition, although BBOA contributions remained relatively limited, it increases from 11% to 17% when OA increased from less than 10 μg m^{-3} to > 25 μg m^{-3}. This may reveal a non-negligible influence of wood burning emissions during early spring pollution episodes.

In summer, OA was also dominated by the two OOA fractions (around 80-85% at all OA-loading bins). The LO-OOA contribution gradually increase from 51 % to 69% as a function of OA mass loadings associated with a significant increase of T (Figure 8 c and g). Other meteorological variables (i.e., RH, WS and BLH) showed relatively stable changes across different OA mass loadings (Figure 8g). These results confirm that high OA concentrations during summer are strongly determined by T-driven biogenic SOA formation processes.

4.4 Potential geographic origins

Figure 9 presents seasonal wind-dependent variations of the POA factors. Wind rose plots (Figure 9a) present the greatest frequency (up to approximate 32%) of winds associated with southwestern wind direction in all seasons. The percentages (about 10-15%) of wind direction from the West-North-East regions are comparable in spring. As presented in Figure 9b, BBOA shows high concentrations associated with the eastern wind sectors, except in summer, which is in agreement with the location of the residential area on the East and West parts of SIRTA. Compared to other seasons, high concentrations of BBOA are also observed linking to western wind sectors in winter, which may imply more intense biomass burning from larger scales during colder months. As discussed above, HOA is a mixed factor with biomass burning aerosols during wintertime, which therefore presents a similar wind-dependent pattern as BBOA (Figure 9 b and c). In spring, summer and fall, HOA presents a distinct pattern with high concentrations associated with northeastern wind sectors from urban area of Paris, suggesting that the short-range transports from the urban Paris area may strongly impact the HOA concentrations at SIRTA.

Figure 10 shows maps of the most probable geographic origins of the two OOA factors for each season based on PSCF analysis. In winter, MO-OOA presents high PSCF values over the Benelux, Germany and Poland, showing a major influence of long-range transport of OA from northeastern sectors. Those results may suggest more intense SOA production and aging processes at regional scale for continental air masses. As a matter of fact, MO-OOA shows wider potential source regions than LO-OOA, which is assessed as fresh SOA and could be mainly formed at more local scale in winter. Moreover, the impact of transport from northeastern regions – hosting intense anthropogenic activities (e.g., industries) - onto MO-OOA concentrations may also support a significant anthropogenic origin for this aged SOA factor.

As shown in Figure 10 c and d, both MO-OOA and LO-OOA present high springtime PSCF values originating from the northeastern regions too, which can participate in pollution episodes frequently observed during this season (Petit et al., 2015; Srivastava et al., 2018b). Therefore, mitigation of VOCs emissions at the regional scale could help to reduce the substantial influence of OA on PM limit value exceedances during this season. Narrower distribution of potential source regions was observed in summer and fall, compared to winter and spring. MO-OOA presents potential source regions mainly from the northeast in summer, while it has a high potential source region originating from the south in fall (Figure 10g).

All these results indicated that significant reduction of the SOA burden in the Paris region does not only require the limitation of local source emissions, but also needs a synergistic control strategy for the regional sources, especially from northeastern European regions. In this respect, they confirmed conclusions reached by previous short-term campaigns (e.g., Sciare et al., 2010; Crippa et al., 2013b; Freutel et al., 2013; Beekman et al., 2015).

5. Conclusions

A comprehensive OA source apportionment has been achieved over the region of Paris from November 2011 to March 2018. 4 factors, comprising HOA, BBOA, MO-OOA and LO-OOA, have been identified and selected to ensure consistency of PMF factor solution over 6 years in this study. Mean annual contributions of these factors to OA were of 11-16 % (HOA), 14-19%

(BBOA), 25-42 % (LO-OOA), and 30-45 % (MO-OOA), respectively. BBOA presented a statistically significant seasonal pattern with highest concentrations during cold months, due to residential wood burning emissions. The contribution of BBOA increased with increasing concentration of OA mass in winter and fall – along with decreasing boundary layer height and wind speed – highlighting the importance of biomass burning emissions for OA pollution under stagnant meteorological conditions. HOA presented temporal variations similar to BBOA in cold months, which was partly related to the fact that wood burning emissions also contributed to HOA burden. BBOA and HOA exhibited very limited (< |-70 ng m^{-3} yr^{-1}|) or not significant trends (at the 5% significance level) during the 6^{+}-years investigated period. These results imply that specific mitigation strategies (e.g., emission control), especially for residential wood burning, are still necessary for substantial improvement of air quality in cold season in the Paris region. Moreover, residential biomass burning emissions could be assumed as an important air-pollution source over western Europe, while such a source remains largely unregulated.

LO-OOA and MO-OOA presented different seasonal variations, reflecting different formation mechanisms and/or precursor sources. LO-OOA displayed a pronounced seasonal cycle, with highest contributions to total OA in summer (50-66 %) and lowest ones in winter (12-19 %). Enhanced LO-OOA production during the warm season was assessed to be mainly driven by biogenic SOA formation. This factor showed no significant long-term trend (p>0.05) for the studied period. MO-OOA presented higher contribution to OA in wintertime (35-51 %) and springtime (32-62 %) than during the rest of the year. PSCF analyses suggested a high probability of MO-OOA long-range transport from northeastern Europe towards the Paris region. MO-OOA displayed a significant (p<0.05) decreasing trend (of about -175 ng m^{-3} yr^{-1}), which might reflect the effect of emission control strategy of anthropogenic SOA precursors at the regional scale over the last decade. However, future work is needed to fully understand chemical properties of these SOA factors corresponding to different origins over different seasons in the Paris region and to quantify the impact of emission control on ambient SOA burden.

Data availability. The data have been presented in the text, table and figures as well as supplement. Additional-related data will be available upon request.

724

725   ***Competing interests.*** The authors declare that they have no conflict of interest.

726

727   ***Author contribution.*** O.F., A.A., and V.G. designed and led the study. Y.Z. conducted the data analyses.
728   J-E.P., F.T., N.B., V.C., T.A., and J.S. provided the field observation. F. C. and A.P. supported the source
729   apportionment analyses. Y.Z. and O.F. interpreted the data, and wrote the manuscript, with inputs
730   from all coauthors.

731

732   ***Acknowledgements.*** This work has been part of the EU-FP7 and H2020 ACTRIS projects (grant
733   agreements no. 262254 and 654109) as well as the COLOSSAL COST action CA16109. It has also been
734   directly supported by the National Center for Scientific Research (CNRS), the French alternatives
735   energies and Atomic Energy Commission (CEA), and the French ministry of Environment through its
736   funding to the reference laboratory for air quality monitoring (LCSQA). Finally, Y. Zhang acknowledges
737   the China Scholarship Council (CSC) for PhD scholarship.

738

References

Aiken, A.C., DeCarlo, P.F., Kroll, J.H., Worsnop, D.R., Huffman, J.A., Docherty, K.S., Ulbrich, I.M., Mohr, C., Kimmel, J.R., Sueper, D., Sun, Y., Zhang, Q., Trimborn, A., Northway, M., Ziemann, P.J., Canagaratna, M.R., Onasch, T.B., Alfarra, M.R., Prévôt, A.S.H., Dommen, J., Duplissy, J., Metzger, A., Baltensperger, U., and Jimenez, J.L. : O/C and OM/OC ratios of primary, secondary, and ambient organic aerosols with high-resolution time-of-flight aerosol mass spectrometer, Environ. Sci. Technol., 42, 4478–4485, 2008.

Alfarra, M. R., Prevot, A. S. H., Szidat, S., Sandradewi, J., Weimer, S., Lanz, V. A., Schreiber, D., Mohr, M., and Baltensperger, U.: Identification of the Mass Spectral Signature of Organic Aerosols from Wood Burning Emissions, Environ. Sci. Technol., 41, 5770-5777, 10.1021/es062289b, 2007.

Bae, M.-S., Demerjian, K. L., and Schwab, J. J.: Seasonal estimation of organic mass to organic carbon in PM2.5 at rural and urban locations in New York state, Atmos. Environ., 40, 7467-7479, https://doi.org/10.1016/j.atmosenv.2006.07.008, 2006.

Baudic, A., Gros, V., Sauvage, S., Locoge, N., Sanchez, O., Sarda-Estève, R., Kalogridis, C., Petit, J. E., Bonnaire, N., Baisnée, D., Favez, O., Albinet, A., Sciare, J., and Bonsang, B.: Seasonal variability and source apportionment of volatile organic compounds (VOCs) in the Paris megacity (France), Atmos. Chem. Phys., 16, 11961-11989, 10.5194/acp-16-11961-2016, 2016.

Beekmann, A. S. H. Prévôt, F. Drewnick, J. Sciare, S. N. Pandis, H. A. C. Denier van der Gon, M. Crippa, F. Freutel, L. Poulain, V. Ghersi, E. Rodriguez, S. Beirle, P. Zotter, S.-L. von der Weiden-Reinmüller, M. Bressi, C. Fountoukis, H. Petetin, S. Szidat, J. Schneider, A. Rosso, I. El Haddad, A. Megaritis, Q.J. Zhang, V. Michoud, J.G. Slowik, S. Moukhtar, P. Kolmonen, A. Stohl1, S. Eckhardt, A. Borbon, V. Gros, N. Marchand, J.L. Jaffrezo, A. Schwarzenboeck, A. Colomb, A. Wiedensohler, S. Borrmann, M. Lawrence, A. Baklanov, U. Baltensperger, In-situ, satellite measurement and model evidence for a dominant regional contribution to fine particulate matter levels in the Paris Megacity, Atmos. Chem. Phys., 15, 9577-9591, 2015.

Bertrand, A., Stefenelli, G., Bruns, E. A., Pieber, S. M., Temime-Roussel, B., Slowik, J. G., Prévôt, A. S. H., Wortham, H., El Haddad, I., and Marchand, N.: Primary emissions and secondary aerosol production potential from woodstoves for residential heating: Influence of the stove technology and combustion efficiency, Atmos. Environ., 169, 65-79, https://doi.org/10.1016/j.atmosenv.2017.09.005, 2017.

Bressi, M., Sciare, J., Ghersi, V., Bonnaire, N., Nicolas, J. B., Petit, J.-E., Moukhtar, S., Rosso, A., Mihalopoulos, N., and Féron, A.: A one-year comprehensive chemical characterisation of fine aerosol (PM$_{2.5}$) at urban, suburban and rural background sites in the region of Paris (France), Atmos. Chem. Phys., 13, 7825-7844, https://doi.org/10.5194/acp-13-7825-2013, 2013.

Bressi, M., Sciare, J., Ghersi, V., Mihalopoulos, N., Petit, J. E., Nicolas, J. B., Moukhtar, S., Rosso, A., Féron, A., Bonnaire, N., Poulakis, E., and Theodosi, C.: Sources and geographical origins of fine aerosols in Paris (France), Atmos. Chem. Phys., 14, 8813-8839, 10.5194/acp-14-8813-2014, 2014.

Boichu, M., Favez, O., Riffault, V., Brogniez, C., Sciare, J., Chiapello, I., Clarisse, L., Zhang, S., Pujol-Söhne, N., Tison, E., Delbarre, H., and Goloub, P.: Large-scale particulate air pollution and chemical fingerprint of volcanic sulfate aerosols from the 2014-15 Holuhraun flood lava eruption of Bárðarbunga volcano (Iceland), Atmos. Chem. Phys. Discuss., 2019, 1-39, 10.5194/acp-2019-228, 2019.

Boucher, O., Randall, D., Artaxo, P., Bretherton, C., Feingold, G., Forster, P., Kerminen, V.-M., Kondo, Y., Liao, H., Lohmann, U., Rasch, P., Satheesh, S. K., Sherwood, S., Stevens, B., and Zhang, X. Y.: Clouds and Aerosols, in: Climate Change 2013: The Physical Science Basis. Contribution of Working Group I to the Fifth Assessment Report of the Intergovernmental Panel on Climate Change, edited by: Stocker, T. F., Qin, D., Plattner, G.-K., Tignor, M., Allen, S. K., Boschung, J., Nauels, A., Xia, Y., Bex, V., and Midgley, P. M., Cambridge University Press, Cambridge, United Kingdom and New York, NY, USA, 571–658, 2013.

Bozzetti, C., El Haddad, I., Salameh, D., Daellenbach, K. R., Fermo, P., Gonzalez, R., Minguillón, M. C., Iinuma, Y., Poulain, L., Elser, M., Müller, E., Slowik, J. G., Jaffrezo, J. L., Baltensperger, U., Marchand, N., and Prévôt, A. S. H.: Organic aerosol source apportionment by offline-AMS over a full year in Marseille, Atmos. Chem. Phys., 17, 8247-8268, 10.5194/acp-17-8247-2017, 2017.

Budisulistiorini, S. H., Li, X., Bairai, S. T., Renfro, J., Liu, Y., Liu, Y. J., McKinney, K. A., Martin, S. T., McNeill, V. F., Pye, H. O. T., Nenes, A., Neff, M. E., Stone, E. A., Mueller, S., Knote, C., Shaw, S. L., Zhang, Z., Gold, A. and Surratt, J. D.: Examining the effects of anthropogenic emissions on isoprene-derived secondary organic aerosol formation during the 2013 Southern Oxidant and Aerosol Study (SOAS) at the Look Rock, Tennessee ground site, Atmos. Chem. Phys., 15(15), 8871–8888, doi:10.5194/acp-15-8871-2015, 2015.

Canagaratna, M. R., Jayne, J. T., Jimenez, J. L., Allan, J. D., Alfarra, M. R., Zhang, Q., Onasch, T. B., Drewnick, F., Coe, H., Middlebrook, A., Delia, A., Williams, L. R., Trimborn, A. M., Northway, M. J., DeCarlo, P. F., Kolb, C. E., Davidovits, P., and Worsnop, D. R.: Chemical and microphysical characterization of ambient aerosols with the aerodyne aerosol mass spectrometer, Mass Spectrom. Rev., 26, 185-222, 10.1002/mas.20115, 2007.

Canagaratna, M. R., Jimenez, J. L., Kroll, J.H., Chen, Q., Kessler, S.H., Massoli, P., Hildebrandt Ruiz, L., Fortner, E., Williams, L.R., Wilson, K.R., Surratt, J.D., Donahue, N.M., Jayne, J. T., and Worsnop, D. R.: Elemental ratio measurements of organic compounds using aerosol mass spectrometry: characterization, improved calibration, and implications, Atmos. Chem. Phys., 15-253-272, doi: 10.5194/acp-15-253-2015, 2015.

Canonaco, F., Crippa, M., Slowik, J. G., Baltensperger, U., and Prévôt, A. S. H.: SoFi, an IGOR-based interface for the efficient use of the generalized multilinear engine (ME-2) for the source apportionment: ME-2 application to aerosol mass spectrometer data, Atmos. Meas. Tech., 6, 3649-3661, 10.5194/amt-6-3649-2013, 2013.

Canonaco, F., Slowik, J. G., Baltensperger, U., and Prévôt, A. S. H.: Seasonal differences in oxygenated organic aerosol composition: implications for emissions sources and factor analysis, Atmos. Chem. Phys., 15, 6993-7002, 10.5194/acp-15-6993-2015, 2015.

Cavalli, F., Viana, M., Yttri, K. E., Genberg, J., and Putaud, J. P.: Toward a standardised thermal-optical protocol for measuring atmospheric organic and elemental carbon: the EUSAAR protocol, Atmos. Meas. Tech., 3, 79-89, 10.5194/amt-3-79-2010, 2010.

CITEPA, édition mars: Inventaire des émissions de polluants atmosphériques en France métropolitaine, format CEE-NU, available at: https://www.citepa.org/images/III-1_Rapports_Inventaires/CEE-NU/UNECE_France_mars2018.pdf (last access: May 2019), 2018.

Crenn, V., Sciare, J., Croteau, P. L., Verlhac, S., Fröhlich, R., Belis, C. A., Aas, W., Äijälä, M., Alastuey, A., Artiñano, B., Baisnée, D., Bonnaire, N., Bressi, M., Canagaratna, M., Canonaco, F., Carbone, C., Cavalli, F., Coz, E., Cubison, M. J., Esser-Gietl, J. K., Green, D. C., Gros, V., Heikkinen, L., Herrmann, H., Lunder, C., Minguillón, M. C., Močnik, G., O'Dowd, C. D., Ovadnevaite, J., Petit, J. E., Petralia, E., Poulain, L., Priestman, M., Riffault, V., Ripoll, A., Sarda-Estève, R., Slowik, J. G., Setyan, A., Wiedensohler, A., Baltensperger, U., Prévôt, A. S. H., Jayne, J. T., and Favez, O.: ACTRIS ACSM intercomparison – Part 1: Reproducibility of concentration and fragment results from 13 individual Quadrupole Aerosol Chemical Speciation Monitors (Q-ACSM) and consistency with co-located instruments, Atmos. Meas. Tech., 8, 5063-5087, 10.5194/amt-8-5063-2015, 2015.

Crippa, M., Canonaco, F., Slowik, J. G., El Haddad, I., DeCarlo, P. F., Mohr, C., Heringa, M. F., Chirico, R., Marchand, N., Temime-Roussel, B., Abidi, E., Poulain, L., Wiedensohler, A., Baltensperger, U., and Prévôt, A. S. H.: Primary and secondary organic aerosol origin by combined gas-particle phase source apportionment, Atmos. Chem. Phys., 13, 8411-8426, 10.5194/acp-13-8411-2013, 2013a.

Crippa, M., DeCarlo, P. F., Slowik, J. G., Mohr, C., Heringa, M. F., Chirico, R., Poulain, L., Freutel, F., Sciare, J., Cozic, J., Di Marco, C. F., Elsasser, M., Nicolas, J. B., Marchand, N., Abidi, E., Wiedensohler, A., Drewnick, F., Schneider, J., Borrmann, S., Nemitz, E., Zimmermann, R., Jaffrezo, J. L., Prévôt, A. S. H., and Baltensperger, U.: Wintertime aerosol chemical composition

842   and source apportionment of the organic fraction in the metropolitan area of Paris, Atmos.
843   Chem. Phys., 13, 961-981, 10.5194/acp-13-961-2013, 2013b.

844 Crippa, M., Canonaco, F., Lanz, V. A., Äijälä, M., Allan, J. D., Carbone, S., Capes, G., Ceburnis, D.,
845   Dall'Osto, M., Day, D. A., DeCarlo, P. F., Ehn, M., Eriksson, A., Freney, E., Hildebrandt Ruiz, L.,
846   Hillamo, R., Jimenez, J. L., Junninen, H., Kiendler-Scharr, A., Kortelainen, A. M., Kulmala, M.,
847   Laaksonen, A., Mensah, A. A., Mohr, C., Nemitz, E., O'Dowd, C., Ovadnevaite, J., Pandis, S. N.,
848   Petäjä, T., Poulain, L., Saarikoski, S., Sellegri, K., Swietlicki, E., Tiitta, P., Worsnop, D. R.,
849   Baltensperger, U., and Prévôt, A. S. H.: Organic aerosol components derived from 25 AMS data
850   sets across Europe using a consistent ME-2 based source apportionment approach, Atmos.
851   Chem. Phys., 14, 6159-6176, 10.5194/acp-14-6159-2014, 2014.

852 Daellenbach, K. R., Kourtchev, I., Vogel, A. L., Bruns, E. A., Jiang, J., Petäjä, T., Jaffrezo, J. L., Aksoyoglu,
853   S., Kalberer, M., Baltensperger, U., El Haddad, I., and Prévôt, A. S. H.: Impact of anthropogenic
854   and biogenic sources on the seasonal variation in the molecular composition of urban organic
855   aerosols: a field and laboratory study using ultra-high-resolution mass spectrometry, Atmos.
856   Chem. Phys., 19, 5973-5991, 10.5194/acp-19-5973-2019, 2019.

857 Daellenbach, K. R., Stefenelli, G., Bozzetti, C., Vlachou, A., Fermo, P., Gonzalez, R., Piazzalunga, A.,
858   Colombi, C., Canonaco, F., Hueglin, C., Kasper-Giebl, A., Jaffrezo, J. L., Bianchi, F., Slowik, J. G.,
859   Baltensperger, U., El-Haddad, I., and Prévôt, A. S. H.: Long-term chemical analysis and organic
860   aerosol source apportionment at nine sites in central Europe: source identification and
861   uncertainty assessment, Atmos. Chem. Phys., 17, 13265-13282, 10.5194/acp-17-13265-2017,
862   2017.

863 Dall'Osto, M., Paglione, M., Decesari, S., Facchini, M. C., O'Dowd, C., Plass-Duellmer, C., and Harrison,
864   R. M.: On the Origin of AMS "Cooking Organic Aerosol" at a Rural Site, Environ. Sci. Technol.,
865   49, 13964-13972, 10.1021/acs.est.5b02922, 2015.

866 Draxler, R. R., and Rolph, G.D.: HYSPLIT (HYbrid Single-Particle Lagrangian Integrated Trajectory) Model
867   Access via NOAA ARL READY Website. NOAA Air Resources Laboratory, Silver Spring, MD.
868   http://www.arl.noaa.gov/ready/hysplit4.html., 2003.

869 Drinovec, L., Močnik, G., Zotter, P., Prévôt, A. S. H., Ruckstuhl, C., Coz, E., Rupakheti, M., Sciare, J.,
870   Müller, T., Wiedensohler, A., and Hansen, A. D. A.: The "dual-spot" Aethalometer: an improved
871   measurement of aerosol black carbon with real-time loading compensation, Atmos. Meas.
872   Tech., 8, 1965-1979, 10.5194/amt-8-1965-2015, 2015.

873 Drinovec, L., Gregorič, A., Zotter, P., Wolf, R., Bruns, E. A., Prévôt, A. S. H., Petit, J. E., Favez, O., Sciare,
874   J., Arnold, I. J., Chakrabarty, R. K., Moosmüller, H., Filep, A., and Močnik, G.: The filter-loading
875   effect by ambient aerosols in filter absorption photometers depends on the coating of the
876   sampled particles, Atmos. Meas. Tech., 10, 1043-1059, 10.5194/amt-10-1043-2017, 2017.

877 Dupont, J.-C., Haeffelin, M., Badosa, J., Elias, T., Favez, O., Petit, J.-E., Meleux, F., Sciare, J., Crenn, V.,
878   and Bonne, J.-L.: Role of the boundary layer dynamics effects on an extreme air pollution event
879   in Paris, Atmos. Environ., 141, 571-579, doi: 10.1016/j.atmosenv.2016.06.061, 2016.

880 EMEP: Air pollution trends in the EMEP region between 1990 and 2012. CCC-report 1/2016, avaialbe
881   at   http://publications.iass-
882   potsdam.de/pubman/item/escidoc:1622889:8/component/escidoc:1622890/1622889.pdf
883   (last access: May 2019), 2016

884 Favez, O., Cachier, H., Sciare, J., Sarda-Estève, R., and Martinon, L.: Evidence for a significant
885   contribution of wood burning aerosols to PM2.5 during the winter season in Paris, France,
886   Atmos. Environ., 43, 3640-3644, https://doi.org/10.1016/j.atmosenv.2009.04.035, 2009.

887 Favez, O., El Haddad, I., Piot, C., Boréave, A., Abidi, E., Marchand, N., Jaffrezo, J.L., Besombes, J.L.,
888   Personnaz, M.B., Sciare, J., Wortham, H., George, C., and D'Anna, B.: Inter-comparison of
889   source apportionment models for the estimation of wood burning aerosols during wintertime
890   in an Alpine city (Grenoble, France), Atmos. Chem. Phys., 10, 5295-5314, 2010.

891 Freney, E., Sellegri, K., Chrit, M., Adachi, K., Brito, J., Waked, A., Borbon, A., Colomb, A., Dupuy, R.,
892   Pichon, J. M., Bouvier, L., Delon, C., Jambert, C., Durand, P., Bourianne, T., Gaimoz, C., Triquet,
893   S., Féron, A., Beekmann, M., Dulac, F., and Sartelet, K.: Aerosol composition and the

contribution of SOA formation over Mediterranean forests, Atmos. Chem. Phys., 18, 7041-7056, 10.5194/acp-18-7041-2018, 2018.

Freney, E., Zhang, Y., Croteau, P., Amodeo, T., Williams, L., Truong, F., Petit, J.-E., Sciare, J., Sarda-Esteve, R., Bonnaire, N., Arumae, T., Aurela, M., Bougiatioti, A., Mihalopoulos, N., Coz, E., Artinano, B., Crenn, V., Elste, T., Heikkinen, L., Poulain, L., Wiedensohler, A., Herrmann, H., Priestman, M., Alastuey, A., Stavroulas, I., Tobler, A., Vasilescu, J., Zanca, N., Canagaratna, M., Carbone, C., Flentje, H., Green, D., Maasikmets, M., Marmureanu, L., Minguillon, M. C., Prevot, A. S. H., Gros, V., Jayne, J., and Favez, O.: The second ACTRIS inter-comparison (2016) for Aerosol Chemical Speciation Monitors (ACSM): Calibration protocols and instrument performance evaluations, Aerosol Sci. Technol., 1-25, 10.1080/02786826.2019.1608901, 2019.

Freutel, F., Schneider, J., Drewnick, F., von der Weiden-Reinmüller, S. L., Crippa, M., Prévôt, A. S. H., Baltensperger, U., Poulain, L., Wiedensohler, A., Sciare, J., Sarda-Estève, R., Burkhart, J. F., Eckhardt, S., Stohl, A., Gros, V., Colomb, A., Michoud, V., Doussin, J. F., Borbon, A., Haeffelin, M., Morille, Y., Beekmann, M., and Borrmann, S.: Aerosol particle measurements at three stationary sites in the megacity of Paris during summer 2009: meteorology and air mass origin dominate aerosol particle composition and size distribution, Atmos. Chem. Phys., 13, 933-959, 10.5194/acp-13-933-2013, 2013.

Fröhlich, R., Crenn, V., Setyan, A., Belis, C. A., Canonaco, F., Favez, O., Riffault, V., Slowik, J. G., Aas, W., Aijälä, M., Alastuey, A., Artiñano, B., Bonnaire, N., Bozzetti, C., Bressi, M., Carbone, C., Coz, E., Croteau, P. L., Cubison, M. J., Esser-Gietl, J. K., Green, D. C., Gros, V., Heikkinen, L., Herrmann, H., Jayne, J. T., Lunder, C. R., Minguillón, M. C., Močnik, G., O'Dowd, C. D., Ovadnevaite, J., Petralia, E., Poulain, L., Priestman, M., Ripoll, A., Sarda-Estève, R., Wiedensohler, A., Baltensperger, U., Sciare, J., and Prévôt, A. S. H.: ACTRIS ACSM intercomparison − Part 2: Intercomparison of ME-2 organic source apportionment results from 15 individual, co-located aerosol mass spectrometers, Atmos. Meas. Tech., 8, 2555-2576, 10.5194/amt-8-2555-2015, 2015b.

Fröhlich, R., Cubison, M. J., Slowik, J. G., Bukowiecki, N., Canonaco, F., Croteau, P. L., Gysel, M., Henne, S., Herrmann, E., Jayne, J. T., Steinbacher, M., Worsnop, D. R., Baltensperger, U., and Prévôt, A. S. H.: Fourteen months of on-line measurements of the non-refractory submicron aerosol at the Jungfraujoch (3580 m a.s.l.) − chemical composition, origins and organic aerosol sources, Atmos. Chem. Phys., 15, 11373-11398, https://doi.org/10.5194/acp-15-11373-2015, 2015a.

Gentner, D. R., Jathar, S. H., Gordon, T. D., Bahreini, R., Day, D. A., El Haddad, I., Hayes, P. L., Pieber, S. M., Platt, S. M., de Gouw, J., Goldstein, A. H., Harley, R. A., Jimenez, J. L., Prévôt, A. S. H., and Robinson, A. L.: Review of Urban Secondary Organic Aerosol Formation from Gasoline and Diesel Motor Vehicle Emissions, Environ. Sci. Technol., 51, 1074-1093, 10.1021/acs.est.6b04509, 2017.

Gilardoni, S., Massoli, P., Paglione, M., Giulianelli, L., Carbone, C., Rinaldi, M., Decesari, S., Sandrini, S., Costabile, F., Gobbi, G. P., Pietrogrande, M. C., Visentin, M., Scotto, F., Fuzzi, S., and Facchini, M. C.: Direct observation of aqueous secondary organic aerosol from biomass-burning emissions, Proc. Natl. Acad. Sci. U. S. A., 113, 10013-10018, 10.1073/pnas.1602212113, 2016.

Goldstein, A. H., Koven, C. D., Heald, C. L., and Fung, I. Y.: Biogenic carbon and anthropogenic pollutants combine to form a cooling haze over the southeastern United States, Proc. Natl. Acad. Sci. U. S. A., 106, 8835-8840, 10.1073/pnas.0904128106, 2009.

Haeffelin, M., Barthès, L., Bock, O., Boitel, C., Bony, S., Bouniol, D., Chepfer, H., Chiriaco, M., Cuesta, J., Delanoë, J., Drobinski, P., Dufresne, J. L., Flamant, C., Grall, M., Hodzic, A., Hourdin, F., Lapouge, F., Lemaître, Y., Mathieu, A., Morille, Y., Naud, C., Noël, V., O'Hirok, W., Pelon, J., Pietras, C., Protat, A., Romand, B., Scialom, G., and Vautard, R.: SIRTA, a ground-based atmospheric observatory for cloud and aerosol research, Ann. Geophys., 23, 253-275, 10.5194/angeo-23-253-2005, 2005.

Hallquist, M., Wenger, J. C., Baltensperger, U., Rudich, Y., Simpson, D., Claeys, M., Dommen, J., Donahue, N. M., George, C., Goldstein, A. H., Hamilton, J. F., Herrmann, H., Hoffmann, T., Iinuma, Y., Jang, M., Jenkin, M. E., Jimenez, J. L., Kiendler-Scharr, A., Maenhaut, W., McFiggans,

946   G., Mentel, T. F., Monod, A., Prévôt, A. S. H., Seinfeld, J. H., Surratt, J. D., Szmigielski, R., and
947   Wildt, J.: The formation, properties and impact of secondary organic aerosol: current and
948   emerging issues, Atmos. Chem. Phys., 9, 5155-5236, 10.5194/acp-9-5155-2009, 2009.
949 Heringa, M. F., DeCarlo, P. F., Chirico, R., Tritscher, T., Dommen, J., Weingartner, E., Richter, R., Wehrle,
950   G., Prévôt, A. S. H., and Baltensperger, U.: Investigations of primary and secondary particulate
951   matter of different wood combustion appliances with a high-resolution time-of-flight aerosol
952   mass spectrometer, Atmos. Chem. Phys., 11, 5945-5957, 10.5194/acp-11-5945-2011, 2011.
953 Hoesly, R. M., Smith, S. J., Feng, L., Klimont, Z., Janssens-Maenhout, G., Pitkanen, T., Seibert, J. J., Vu,
954   L., Andres, R. J., Bolt, R. M., Bond, T. C., Dawidowski, L., Kholod, N., Kurokawa, J. I., Li, M., Liu,
955   L., Lu, Z., Moura, M. C. P., O'Rourke, P. R., and Zhang, Q.: Historical (1750–2014) anthropogenic
956   emissions of reactive gases and aerosols from the Community Emissions Data System (CEDS),
957   Geosci. Model Dev., 11, 369-408, 10.5194/gmd-11-369-2018, 2018.
958 Jayne, J. T., Leard, D. C., Zhang, X., Davidovits, P., Smith, K. A., Kolb, C. E., and Worsnop, D. R.:
959   Development of an Aerosol Mass Spectrometer for Size and Composition Analysis of
960   Submicron Particles, Aerosol Sci. Technol., 33, 49-70, 10.1080/027868200410840, 2000.
961 Jimenez, J. L., Canagaratna, M. R., Donahue, N. M., Prevot, A. S. H., Zhang, Q., Kroll, J. H., DeCarlo, P.
962   F., Allan, J. D., Coe, H., Ng, N. L., Aiken, A. C., Docherty, K. S., Ulbrich, I. M., Grieshop, A. P.,
963   Robinson, A. L., Duplissy, J., Smith, J. D., Wilson, K. R., Lanz, V. A., Hueglin, C., Sun, Y. L., Tian,
964   J., Laaksonen, A., Raatikainen, T., Rautiainen, J., Vaattovaara, P., Ehn, M., Kulmala, M.,
965   Tomlinson, J. M., Collins, D. R., Cubison, M. J., Dunlea, J., Huffman, J. A., Onasch, T. B., Alfarra,
966   M. R., Williams, P. I., Bower, K., Kondo, Y., Schneider, J., Drewnick, F., Borrmann, S., Weimer,
967   S., Demerjian, K., Salcedo, D., Cottrell, L., Griffin, R., Takami, A., Miyoshi, T., Hatakeyama, S.,
968   Shimono, A., Sun, J. Y., Zhang, Y. M., Dzepina, K., Kimmel, J. R., Sueper, D., Jayne, J. T., Herndon,
969   S. C., Trimborn, A. M., Williams, L. R., Wood, E. C., Middlebrook, A. M., Kolb, C. E.,
970   Baltensperger, U., and Worsnop, D. R.: Evolution of Organic Aerosols in the Atmosphere,
971   Science, 326, 1525-1529, 10.1126/science.1180353, 2009.
972 Kroll, J. H., and Seinfeld, J. H.: Chemistry of secondary organic aerosol: Formation and evolution of low-
973   volatility organics in the atmosphere, Atmos. Environ., 42, 3593-3624,
974   10.1016/j.atmosenv.2008.01.003, 2008.
975 Kruskal, W. H., and Wallis, W. A.: Use of Ranks in One-Criterion Variance Analysis, J. Am. Stat. Assoc.,
976   47, 583-621, 10.2307/2280779, 1952.
977 Lanz, V. A., Alfarra, M. R., Baltensperger, U., Buchmann, B., Hueglin, C., and Prévôt, A. S. H.: Source
978   apportionment of submicron organic aerosols at an urban site by factor analytical modelling
979   of aerosol mass spectra, Atmos. Chem. Phys., 7, 1503-1522, 10.5194/acp-7-1503-2007, 2007.
980 Lanz, V. A., Prévôt, A. S. H., Alfarra, M. R., Weimer, S., Mohr, C., DeCarlo, P. F., Gianini, M. F. D., Hueglin,
981   C., Schneider, J., Favez, O., D'Anna, B., George, C., and Baltensperger, U.: Characterization of
982   aerosol chemical composition with aerosol mass spectrometry in Central Europe: an overview,
983   Atmos. Chem. Phys., 10, 10453-10471, 10.5194/acp-10-10453-2010, 2010.
984 Leaitch, W. R., Macdonald, A. M., Brickell, P. C., Liggio, J., Sjostedt, S. J., Vlasenko, A., Bottenheim, J.
985   W., Huang, L., Li, S.-M., Liu, P. S. K., Toom-Sauntry, D., Hayden, K. A., Sharma, S., Shantz, N. C.,
986   Wiebe, H. A., Zhang, W., Abbatt, J. P. D., Slowik, J. G., Chang, R. Y. W., Russell, L. M., Schwartz,
987   R. E., Takahama, S., Jayne, J. T., and Ng, N. L.: Temperature response of the submicron organic
988   aerosol from temperate forests, Atmos. Environ., 45, 6696-6704,
989   https://doi.org/10.1016/j.atmosenv.2011.08.047, 2011.
990 Li, Y. J., Sun, Y., Zhang, Q., Li, X., Li, M., Zhou, Z., and Chan, C. K.: Real-time chemical characterization
991   of atmospheric particulate matter in China: A review, Atmos. Environ., 158, 270-304,
992   https://doi.org/10.1016/j.atmosenv.2017.02.027, 2017.
993 Lin, C., Huang, R.-J., Ceburnis, D., Buckley, P., Preissler, J., Wenger, J., Rinaldi, M., Facchini, M. C.,
994   O᾽Dowd, C., and Ovadnevaite, J.: Extreme air pollution from residential solid fuel burning,
995   Nature Sustainability, 1, 512-517, 10.1038/s41893-018-0125-x, 2018.
996 Liu, P. S. K., Deng, R., Smith, K. A., Williams, L. R., Jayne, J. T., Canagaratna, M. R., Moore, K., Onasch,
997   T. B., Worsnop, D. R., and Deshler, T.: Transmission Efficiency of an Aerodynamic Focusing Lens

998   System: Comparison of Model Calculations and Laboratory Measurements for the Aerodyne
999   Aerosol Mass Spectrometer, Aerosol Sci. Technol., 41, 721-733, 10.1080/02786820701422278,
1000   2007.
1001 Middlebrook, A. M., Bahreini, R., Jimenez, J. L., and Canagaratna, M. R.: Evaluation of Composition-
1002   Dependent Collection Efficiencies for the Aerodyne Aerosol Mass Spectrometer using Field
1003   Data, Aerosol Sci. Technol., 46, 258–271, https://doi.org/10.1080/02786826.2011.620041,
1004   2012.
1005 Mohr, C., DeCarlo, P. F., Heringa, M. F., Chirico, R., Slowik, J. G., Richter, R., Reche, C., Alastuey, A.,
1006   Querol, X., Seco, R., Peñuelas, J., Jiménez, J. L., Crippa, M., Zimmermann, R., Baltensperger, U.,
1007   and Prévôt, A. S. H.: Identification and quantification of organic aerosol from cooking and other
1008   sources in Barcelona using aerosol mass spectrometer data, Atmos. Chem. Phys., 12, 1649-
1009   1665, 10.5194/acp-12-1649-2012, 2012.
1010 Mann, H. B.: Nonparametric Tests Against Trend, Econometrica, 13, 245-259, 10.2307/1907187, 1945.
1011 Ng, N. L., Canagaratna, M. R., Zhang, Q., Jimenez, J. L., Tian, J., Ulbrich, I. M., Kroll, J. H., Docherty, K.
1012   S., Chhabra, P. S., Bahreini, R., Murphy, S. M., Seinfeld, J. H., Hildebrandt, L., Donahue, N. M.,
1013   DeCarlo, P. F., Lanz, V. A., Prévôt, A. S. H., Dinar, E., Rudich, Y., and Worsnop, D. R.: Organic
1014   aerosol components observed in Northern Hemispheric datasets from Aerosol Mass
1015   Spectrometry, Atmos. Chem. Phys., 10, 4625-4641, 10.5194/acp-10-4625-2010, 2010.
1016 Ng, N. L., Canagaratna, M. R., Jimenez, J. L., Chhabra, P. S., Seinfeld, J. H., and Worsnop, D. R.: Changes
1017   in organic aerosol composition with aging inferred from aerosol mass spectra, Atmos. Chem.
1018   Phys., 11, 6465-6474, 10.5194/acp-11-6465-2011, 2011a.
1019 Ng, N. L., Herndon, S. C., Trimborn, A., Canagaratna, M. R., Croteau, P. L., Onasch, T. B., Sueper, D.,
1020   Worsnop, D. R., Zhang, Q., Sun, Y. L., and Jayne, J. T.: An Aerosol Chemical Speciation Monitor
1021   (ACSM) for Routine Monitoring of the Composition and Mass Concentrations of Ambient
1022   Aerosol, Aerosol Sci. Technol., 45, 780-794, 10.1080/02786826.2011.560211, 2011b.
1023 Nozière, B., Kalberer, M., Claeys, M., Allan, J., D'Anna, B., Decesari, S., Finessi, E., Glasius, M., Grgić, I.,
1024   Hamilton, J. F., Hoffmann, T., Iinuma, Y., Jaoui, M., Kahnt, A., Kampf, C. J., Kourtchev, I.,
1025   Maenhaut, W., Marsden, N., Saarikoski, S., Schnelle-Kreis, J., Surratt, J. D., Szidat, S., Szmigielski,
1026   R., and Wisthaler, A.: The Molecular Identification of Organic Compounds in the Atmosphere:
1027   State of the Art and Challenges, Chem. Rev., 115, 3919-3983, 10.1021/cr5003485, 2015.
1028 Paatero, P., and Tapper, U.: Positive matrix factorization: A non-negative factor model with optimal
1029   utilization of error estimates of data values, Environmetrics, 5, 111-126,
1030   doi:10.1002/env.3170050203, 1994.
1031 Paatero, P.: The Multilinear Engine—A Table-Driven, Least Squares Program for Solving Multilinear
1032   Problems, Including the n-Way Parallel Factor Analysis Model, J. Comput. Graph. Stat., 8, 854-
1033   888, 10.1080/10618600.1999.10474853, 1999.
1034 Pandolfi, M., Alados-Arboledas, L., Alastuey, A., Andrade, M., Angelov, C., Artiñano, B., Backman, J.,
1035   Baltensperger, U., Bonasoni, P., Bukowiecki, N., Collaud Coen, M., Conil, S., Coz, E., Crenn, V.,
1036   Dudoitis, V., Ealo, M., Eleftheriadis, K., Favez, O., Fetfatzis, P., Fiebig, M., Flentje, H., Ginot, P.,
1037   Gysel, M., Henzing, B., Hoffer, A., Holubova Smejkalova, A., Kalapov, I., Kalivitis, N., Kouvarakis,
1038   G., Kristensson, A., Kulmala, M., Lihavainen, H., Lunder, C., Luoma, K., Lyamani, H., Marinoni,
1039   A., Mihalopoulos, N., Moerman, M., Nicolas, J., O'Dowd, C., Petäjä, T., Petit, J. E., Pichon, J. M.,
1040   Prokopciuk, N., Putaud, J. P., Rodríguez, S., Sciare, J., Sellegri, K., Swietlicki, E., Titos, G., Tuch,
1041   T., Tunved, P., Ulevicius, V., Vaishya, A., Vana, M., Virkkula, A., Vratolis, S., Weingartner, E.,
1042   Wiedensohler, A., and Laj, P.: A European aerosol phenomenology – 6: scattering properties
1043   of atmospheric aerosol particles from 28 ACTRIS sites, Atmos. Chem. Phys., 18, 7877-7911,
1044   10.5194/acp-18-7877-2018, 2018.
1045 Petit, J. E., Favez, O., Sciare, J., Canonaco, F., Croteau, P., Močnik, G., Jayne, J., Worsnop, D., and Leoz-
1046   Garziandia, E.: Submicron aerosol source apportionment of wintertime pollution in Paris,
1047   France by double positive matrix factorization (PMF^2) using an aerosol chemical
1048   speciation monitor (ACSM) and a multi-wavelength Aethalometer, Atmos. Chem. Phys., 14,
1049   13773-13787, 10.5194/acp-14-13773-2014, 2014.

1050   Petit, J. E., Favez, O., Sciare, J., Crenn, V., Sarda-Estève, R., Bonnaire, N., Močnik, G., Dupont, J. C.,
1051   Haeffelin, M., and Leoz-Garziandia, E.: Two years of near real-time chemical composition of
1052   submicron aerosols in the region of Paris using an Aerosol Chemical Speciation Monitor (ACSM)
1053   and a multi-wavelength Aethalometer, Atmos. Chem. Phys., 15, 2985-3005, 10.5194/acp-15-
1054   2985-2015, 2015.
1055   Petit, J. E., Favez, O., Albinet, A., and Canonaco, F.: A user-friendly tool for comprehensive evaluation
1056   of the geographical origins of atmospheric pollution: Wind and trajectory analyses, Environ.
1057   Modell. Softw., 88, 183-187, http://dx.doi.org/10.1016/j.envsoft.2016.11.022, 2017.
1058   Pohlert, T.: Package 'trend', 2018.
1059   Polissar, A. V., Hopke, P. K., Paatero, P., Kaufmann, Y. J., Hall, D. K., Bodhaine, B. A., Dutton, E. G., and
1060   Harris, J. M.: The aerosol at Barrow, Alaska: long-term trends and source locations, Atmos.
1061   Environ., 33, 2441-2458, https://doi.org/10.1016/S1352-2310(98)00423-3, 1999.
1062   Rattanavaraha, W., Canagaratna, M. R., Budisulistiorini, S. H., Croteau, P. L., Baumann, K., Canonaco,
1063   F., Prevot, A. S. H., Edgerton, E. S., Zhang, Z., Jayne, J. T., Worsnop, D. R., Gold, A., Shaw, S. L.,
1064   and Surratt, J. D.: Source apportionment of submicron organic aerosol collected from Atlanta,
1065   Georgia, during 2014–2015 using the aerosol chemical speciation monitor (ACSM), Atmos.
1066   Environ., 167, 389–402, 2017.
1067   Reyes-Villegas, E., Green, D. C., Priestman, M., Canonaco, F., Coe, H., Prévôt, A. S. H., and Allan, J. D.:
1068   Organic aerosol source apportionment in London 2013 with ME-2: exploring the solution space
1069   with annual and seasonal analysis, Atmos. Chem. Phys., 16, 15545-15559, 10.5194/acp-16-
1070   15545-2016, 2016.
1071   Saleh, R., Robinson, E. S., Tkacik, D. S., Ahern, A. T., Liu, S., Aiken, A. C., Sullivan, R. C., Presto, A. A.,
1072   Dubey, M. K., Yokelson, R. J., Donahue, N. M., and Robinson, A. L.: Brownness of organics in
1073   aerosols from biomass burning linked to their black carbon content, Nature Geoscience, 7, 647,
1074   2014.
1075   Sandradewi, J., Prévôt, A. S. H., Szidat, S., Perron, N., Alfarra, M. R., Lanz, V. A., Weingartner, E., and
1076   Baltensperger, U.: Using Aerosol Light Absorption Measurements for the Quantitative
1077   Determination of Wood Burning and Traffic Emission Contributions to Particulate Matter,
1078   Environ. Sci. Technol., 42, 3316-3323, 10.1021/es702253m, 2008.
1079   Schlag, P., Kiendler-Scharr, A., Blom, M. J., Canonaco, F., Henzing, J. S., Moerman, M., Prévôt, A. S. H.,
1080   and Holzinger, R.: Aerosol source apportionment from 1-year measurements at the CESAR
1081   tower in Cabauw, the Netherlands, Atmos. Chem. Phys., 16, 8831-8847, 10.5194/acp-16-8831-
1082   2016, 2016.
1083   Schurgers, G., Arneth, A., Holzinger, R., and Goldstein, A. H.: Process-based modelling of biogenic
1084   monoterpene emissions combining production and release from storage, Atmos. Chem. Phys.,
1085   9, 3409-3423, 10.5194/acp-9-3409-2009, 2009.
1086   Sciare, J., d'Argouges, O., Zhang, Q. J., Sarda-Estève, R., Gaimoz, C., Gros, V., Beekmann, M., and
1087   Sanchez, O.: Comparison between simulated and observed chemical composition of fine
1088   aerosols in Paris (France) during springtime: contribution of regional versus continental
1089   emissions, Atmos. Chem. Phys., 10, 11987-12004, 10.5194/acp-10-11987-2010, 2010.
1090   Sciare, J., d'Argouges, O., Sarda-Estève, R., Gaimoz, C., Dolgorouky, C., Bonnaire, N., Favez, O., Bonsang,
1091   B., and Gros, V.: Large contribution of water-insoluble secondary organic aerosols in the region
1092   of Paris (France) during wintertime, J. Geophys. Res. Atmos., 116, doi:10.1029/2011JD015756,
1093   2011.
1094   Sen, P. K.: Estimates of the Regression Coefficient Based on Kendall's Tau, J. Am. Stat. Assoc., 63, 1379-
1095   1389, 10.2307/2285891, 1968.
1096   Shapiro, S. S., and Wilk, M. B.: An Analysis of Variance Test for Normality (Complete Samples),
1097   Biometrika, 52, 591-611, 10.2307/2333709, 1965.
1098   Shrivastava, M., Cappa, C. D., Fan, J., Goldstein, A. H., Guenther, A. B., Jimenez, J. L., Kuang, C., Laskin,
1099   A., Martin, S. T., Ng, N. L., Petaja, T., Pierce, J. R., Rasch, P. J., Roldin, P., Seinfeld, J. H., Shilling,
1100   J., Smith, J. N., Thornton, J. A., Volkamer, R., Wang, J., Worsnop, D. R., Zaveri, R. A., Zelenyuk,
1101   A., and Zhang, Q.: Recent advances in understanding secondary organic aerosol: Implications

for global climate forcing, Reviews of Geophysics, 55, 509-559, doi:10.1002/2016RG000540, 2017.

Srivastava, D., Favez, O., Perraudin, E., Villenave, E., and Albinet, A.: Comparison of Measurement-Based Methodologies to Apportion Secondary Organic Carbon (SOC) in PM2.5: A Review of Recent Studies, Atmosphere, 9, 452, 2018a.

Srivastava, D., Favez, O., Bonnaire, N., Lucarelli, F., Haeffelin, M., Perraudin, E., Gros, V., Villenave, E., and Albinet, A.: Speciation of organic fractions does matter for aerosol source apportionment. Part 2: Intensive short-term campaign in the Paris area (France), Sci. Total Environ., 634, 267-278, https://doi.org/10.1016/j.scitotenv.2018.03.296, 2018b.

Srivastava, D., Daellenbach, K.R., Zhang, Y., Bonnaire, N., Chazeau, B., Perraudin, E., Gros, V., Villenave, E., Prévôt, A.S.H., El Haddad, I., Favez, O., and Albinet, A.: Comparison of different methodologies to discriminate between primary and secondary organic aerosols, Sci. Total Environ., 690, 944-955, 2019.

Stavroulas, I., Bougiatioti, A., Grivas, G., Paraskevopoulou, D., Tsagkaraki, M., Zarmpas, P., Liakakou, E., Gerasopoulos, E., and Mihalopoulos, N.: Sources and processes that control the submicron organic aerosol composition in an urban Mediterranean environment (Athens): a high temporal-resolution chemical composition measurement study, Atmos. Chem. Phys., 19, 901-919, 10.5194/acp-19-901-2019, 2019.

Stein, A.F., Draxler, R.R., Rolph, G.D., Stunder, B.J.B., Cohen, M.D., Ngan, F.: NOAA's HYSPLIT atmospheric transport and dispersion modeling System. Bull. Am. Meteorol. Soc. 96 (12), 2059e2077. http://dx.doi.org/10.1175/BAMS-D-14-00110.1, 2015.

Sun, Y. L., Zhang, Q., Schwab, J. J., Demerjian, K. L., Chen, W. N., Bae, M. S., Hung, H. M., Hogrefe, O., Frank, B., Rattigan, O. V., and Lin, Y. C.: Characterization of the sources and processes of organic and inorganic aerosols in New York city with a high-resolution time-of-flight aerosol mass apectrometer, Atmos. Chem. Phys., 11, 1581-1602, 10.5194/acp-11-1581-2011, 2011.

Sun, Y., Wang, Z., Dong, H., Yang, T., Li, J., Pan, X., Chen, P., and Jayne, J. T.: Characterization of summer organic and inorganic aerosols in Beijing, China with an Aerosol Chemical Speciation Monitor, Atmos. Environ., 51, 250-259, https://doi.org/10.1016/j.atmosenv.2012.01.013, 2012.

Sun, Y., Xu, W., Zhang, Q., Jiang, Q., Canonaco, F., Prévôt, A. S. H., Fu, P., Li, J., Jayne, J., Worsnop, D. R., and Wang, Z.: Source apportionment of organic aerosol from 2-year highly time-resolved measurements by an aerosol chemical speciation monitor in Beijing, China, Atmos. Chem. Phys., 18, 8469-8489, 10.5194/acp-18-8469-2018, 2018.

Tiitta, P., Leskinen, A., Hao, L., Yli-Pirilä, P., Kortelainen, M., Grigonyte, J., Tissari, J., Lamberg, H., Hartikainen, A., Kuuspalo, K., Kortelainen, A. M., Virtanen, A., Lehtinen, K. E. J., Komppula, M., Pieber, S., Prévôt, A. S. H., Onasch, T. B., Worsnop, D. R., Czech, H., Zimmermann, R., Jokiniemi, J., and Sippula, O.: Transformation of logwood combustion emissions in a smog chamber: formation of secondary organic aerosol and changes in the primary organic aerosol upon daytime and nighttime aging, Atmos. Chem. Phys., 16, 13251-13269, 10.5194/acp-16-13251-2016, 2016.

Ulbrich, I. M., Canagaratna, M. R., Zhang, Q., Worsnop, D. R., and Jimenez, J. L.: Interpretation of organic components from Positive Matrix Factorization of aerosol mass spectrometric data, Atmos. Chem. Phys., 9, 2891-2918, 10.5194/acp-9-2891-2009, 2009.

Waked, A., Favez, O., Alleman, L. Y., Piot, C., Petit, J. E., Delaunay, T., Verlinden, E., Golly, B., Besombes, J. L., Jaffrezo, J. L., and Leoz-Garziandia, E.: Source apportionment of PM10 in a north-western Europe regional urban background site (Lens, France) using positive matrix factorization and including primary biogenic emissions, Atmos. Chem. Phys., 14, 3325-3346, 10.5194/acp-14-3325-2014, 2014.

Xu, L., Guo, H., Boyd, C. M., Klein, M., Bougiatioti, A., Cerully, K. M., Hite, J. R., Isaacman-VanWertz, G., Kreisberg, N. M., Knote, C., Olson, K., Koss, A., Goldstein, A. H., Hering, S. V., de Gouw, J., Baumann, K., Lee, S.-H., Nenes, A., Weber, R. J., and Ng, N. L.: Effects of anthropogenic emissions on aerosol formation from isoprene and monoterpenes in the southeastern United States, Proc. Natl. Acad. Sci. U. S. A., 112, 37-42, 10.1073/pnas.1417609112, 2015.

1154 Xu, W., Han, T., Du, W., Wang, Q., Chen, C., Zhao, J., Zhang, Y., Li, J., Fu, P., Wang, Z., Worsnop, D. R.,
1155   and Sun, Y.: Effects of Aqueous-Phase and Photochemical Processing on Secondary Organic
1156   Aerosol Formation and Evolution in Beijing, China, Environ. Sci. Technol., 51, 762-770,
1157   10.1021/acs.est.6b04498, 2017.
1158 Zanatta, M., Gysel, M., Bukowiecki, N., Müller, T., Weingartner, E., Areskoug, H., Fiebig, M., Yttri, K. E.,
1159   Mihalopoulos, N., Kouvarakis, G., Beddows, D., Harrison, R. M., Cavalli, F., Putaud, J. P.,
1160   Spindler, G., Wiedensohler, A., Alastuey, A., Pandolfi, M., Sellegri, K., Swietlicki, E., Jaffrezo, J.
1161   L., Baltensperger, U., and Laj, P.: A European aerosol phenomenology-5: Climatology of black
1162   carbon optical properties at 9 regional background sites across Europe, Atmos. Environ., 145,
1163   346-364, https://doi.org/10.1016/j.atmosenv.2016.09.035, 2016.
1164 Zhang, Q., Jimenez, J. L., Canagaratna, M. R., Allan, J. D., Coe, H., Ulbrich, I., Alfarra, M. R., Takami, A.,
1165   Middlebrook, A. M., Sun, Y. L., Dzepina, K., Dunlea, E., Docherty, K., DeCarlo, P. F., Salcedo, D.,
1166   Onasch, T., Jayne, J. T., Miyoshi, T., Shimono, A., Hatakeyama, S., Takegawa, N., Kondo, Y.,
1167   Schneider, J., Drewnick, F., Borrmann, S., Weimer, S., Demerjian, K., Williams, P., Bower, K.,
1168   Bahreini, R., Cottrell, L., Griffin, R. J., Rautiainen, J., Sun, J. Y., Zhang, Y. M., and Worsnop, D. R.:
1169   Ubiquity and dominance of oxygenated species in organic aerosols in anthropogenically-
1170   influenced Northern Hemisphere midlatitudes, Geophys. Res. Lett., 34,
1171   doi:10.1029/2007GL029979, 2007.
1172 Zhang, Q., Jimenez, J. L., Canagaratna, M. R., Ulbrich, I. M., Ng, N. L., Worsnop, D. R., and Sun, Y.:
1173   Understanding atmospheric organic aerosols via factor analysis of aerosol mass spectrometry:
1174   a review, Anal. Bioanal. Chem., 401, 3045-3067, 10.1007/s00216-011-5355-y, 2011.
1175 Zhang, Y. J., Tang, L. L., Wang, Z., Yu, H. X., Sun, Y. L., Liu, D., Qin, W., Canonaco, F., Prévôt, A. S. H.,
1176   Zhang, H. L., and Zhou, H. C.: Insights into characteristics, sources, and evolution of submicron
1177   aerosols during harvest seasons in the Yangtze River delta region, China, Atmos. Chem. Phys.,
1178   15, 1331-1349, 10.5194/acp-15-1331-2015, 2015.
1179 Zhang, Y., Tang, L., Sun, Y., Favez, O., Canonaco, F., Albinet, A., Couvidat, F., Liu, D., Jayne, J. T., Wang,
1180   Z., Croteau, P. L., Canagaratna, M. R., Zhou, H., Prévôt, A. S. H. and Worsnop, D. R.: Limited
1181   formation of isoprene epoxydiols–derived secondary organic aerosol (IEPOX-SOA) under NOx-
1182   rich environments in Eastern China, Geophys. Res. Lett., 2016GL072368,
1183   doi:10.1002/2016GL072368, 2017.
1184 Zhang, Y., Favez, O., Canonaco, F., Liu, D., Mocnik, G., Amodeo, T., Sciare, J., Prévôt, A. S. H., Gros, V.,
1185   and Albinet, A.: Evidence of major secondary organic aerosol contribution to lensing effect
1186   black carbon absorption enhancement, npj Climate and Atmospheric Science, 1, 47,
1187   doi:10.1038/s41612-018-0056-2, 2018.
1188 Zhou, S., Collier, S., Jaffe, D. A., Briggs, N. L., Hee, J., Sedlacek III, A. J., Kleinman, L., Onasch, T. B., and
1189   Zhang, Q.: Regional influence of wildfires on aerosol chemistry in the western US and insights
1190   into atmospheric aging of biomass burning organic aerosol, Atmos. Chem. Phys., 17, 2477-
1191   2493, https://doi.org/10.5194/acp-17-2477-2017, 2017.
1192 Zotter, P., Herich, H., Gysel, M., El-Haddad, I., Zhang, Y., Močnik, G., Hüglin, C., Baltensperger, U., Szidat,
1193   S., and Prévôt, A. S. H.: Evaluation of the absorption Ångström exponents for traffic and wood
1194   burning in the Aethalometer-based source apportionment using radiocarbon measurements
1195   of ambient aerosol, Atmos. Chem. Phys., 17, 4229-4249, 10.5194/acp-17-4229-2017, 2017.
1196

1197 **Table 1.** Annual average mass concentration of OA factors, secondary inorganic aerosols (sulfate,
1198 nitrate, and ammonium), and eBC components.

Year	Mass concentration ($\mu g\ m^{-3}$)								
	POA factors		SOA factors		secondary inorganic aerosols			black carbon	
	HOA	BBOA	LO-OOA	MO-OOA	SO_4	NO_3	NH_4	eBC_{ff}	eBC_{wb}
2012	1.01	1.19	1.60	2.48	1.24	3.58	1.71	0.37	0.14
2013	0.82	1.08	2.78	1.99	2.10	4.02	1.75	0.45	0.15
2014	0.57	0.70	1.20	1.67	0.75	2.37	1.03	0.35	0.17
2015	0.51	0.61	1.36	2.01	0.72	2.62	0.91	0.30	0.15
2016	0.60	0.78	1.65	1.28	1.12	2.20	0.98	0.40	0.17
2017	0.64	0.73	1.50	1.49	1.27	1.87	0.95	0.27	0.14

1199
1200

1201
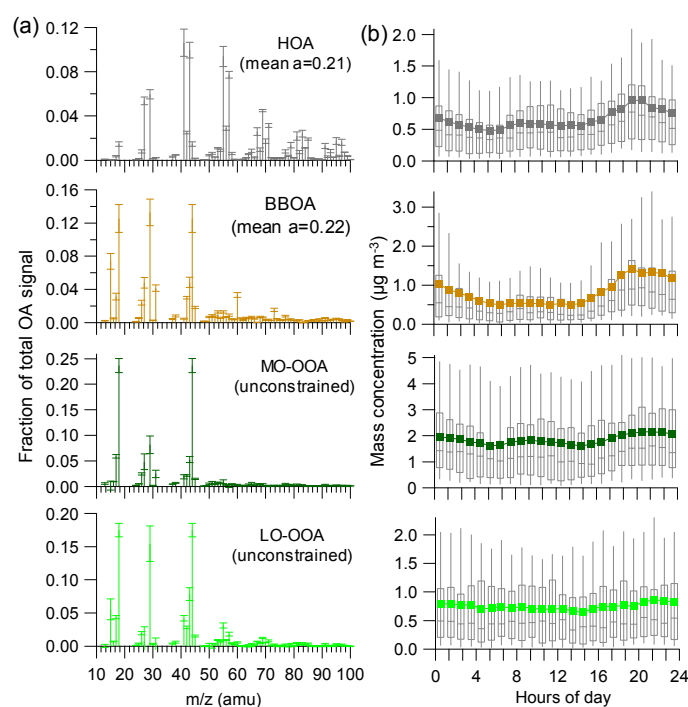
1202 **Figure 1.** Mass spectra (a) and diel variations (b) of four OA factors obtained from the 4-factor
1203 solution of ME-2 runs for winter 2017-2018. In (a), error bars in each plot present 1 standard
1204 deviation. Stick lines indicate average values over all selected ME-2 runs. Averaged a-values
1205 for the constrained factors during the ME-2 runs are also shown. In (b), the upper and lower
1206 boundaries of boxes indicate the 75th and 25th percentiles; the vertical lines within the box
1207 correspond to median values; the whiskers above and below boxes refer to 95th and 10th
1208 percentiles; and solid colored lines represent mean values.

1209

1210
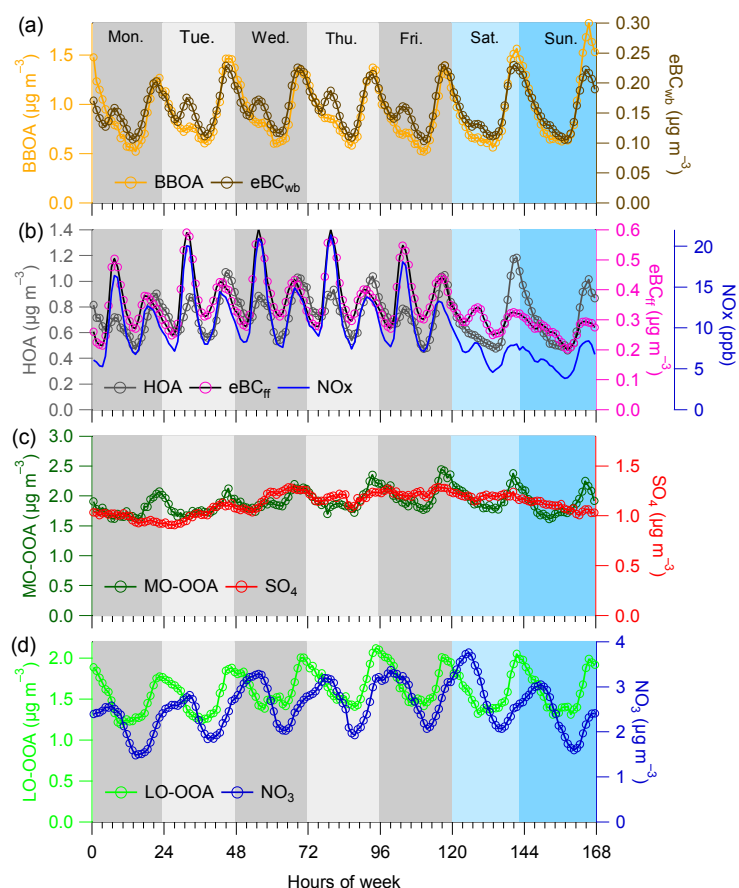
Figure 2. Weekly cycles averaged for the entire period of study for (a) HOA, (b) BBOA, (c) MO-OOA and (d) LO-OOA, along with possible external tracers (eBC$_{wb}$, eBC$_{ff}$ and NO$_x$, sulfate, and nitrate, respectively). Weekdays are colored (every 24 h) in different gray and weekend days in different blue.

1211

1212

1213

1214

1215

1216
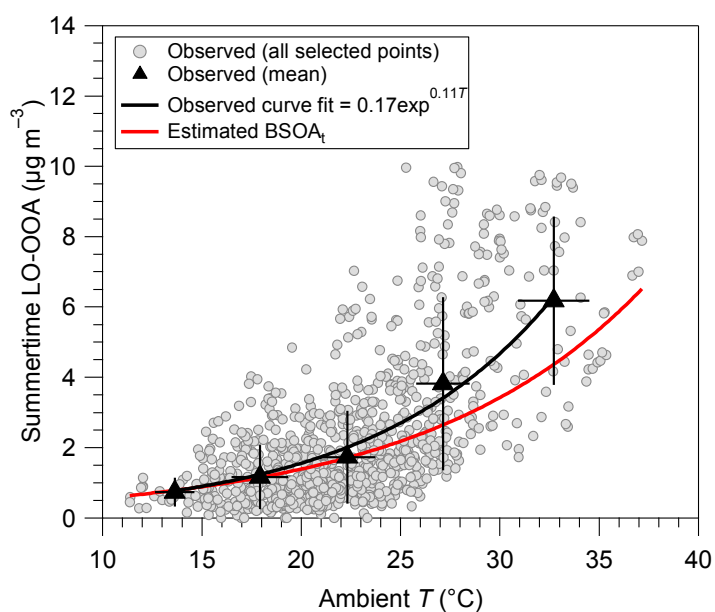
Figure 3. Temperature dependence of summertime LO-OOA obtained from observation and observationally constrained calculation based on biogenic terpene emissions model (Schurgers et al., 2009; Leaitch et al., 2011).

1217

1218

1219

1220

1221
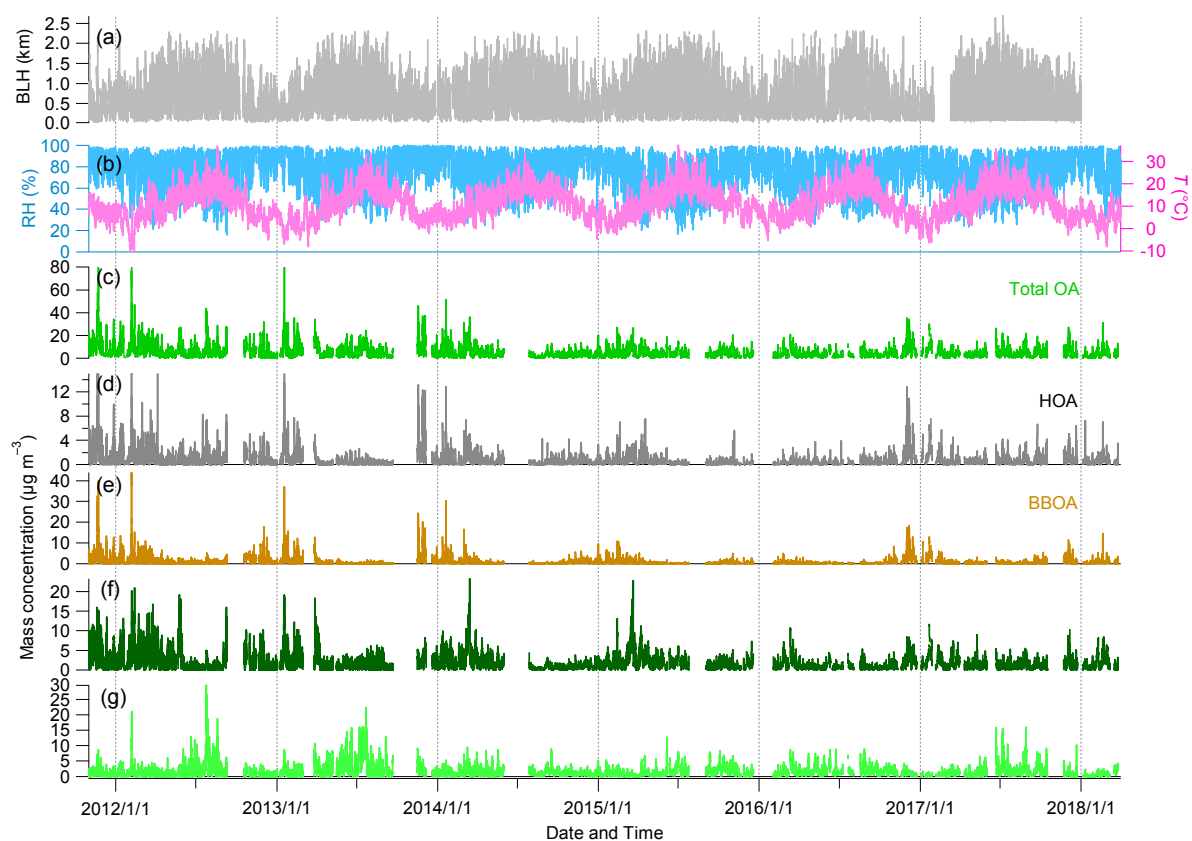
Figure 4. Timeseries of meteorological parameters, i.e., (a) boundary layer height (BLH); and

(b) relative humidity (RH) and temperature (*T*), and mass concentrations of (c) total OA and

four OA PMF factors, i.e., (d) HOA, (e) BBOA, (f) MO-OOA, and (g) LO-OOA.

1225

1226
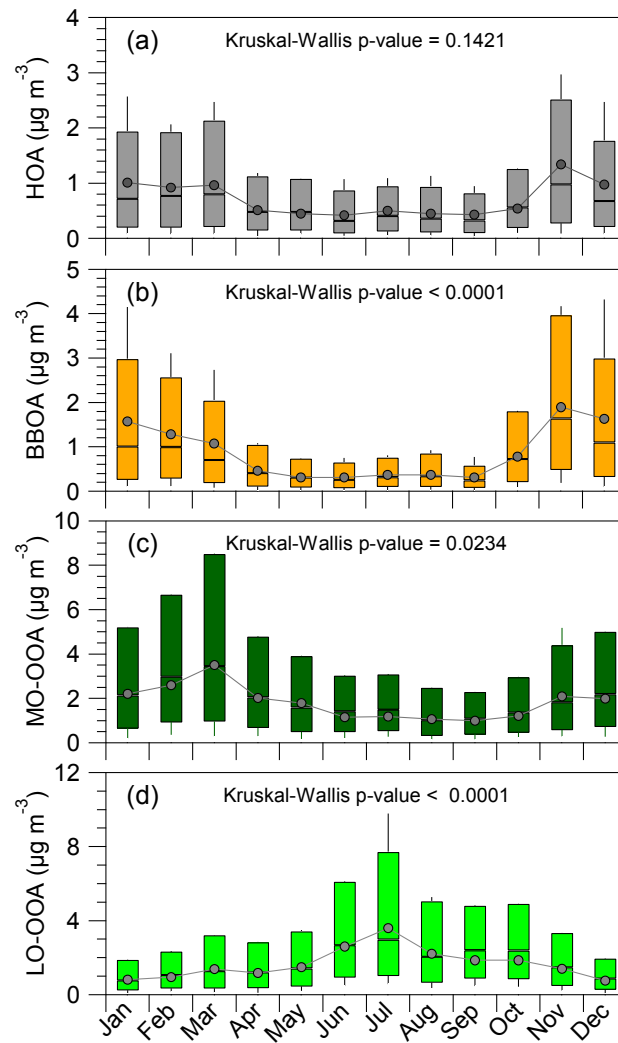
1227   **Figure 5.** Monthly variations of the four OA factors and associated Kruskal-Wallis p-value for

1228   detecting seasonality. The box plots describe the different percentiles (10th, 25th, 50th, 75th,

1229   and 90th) and the mean (gray solid circle).

1230

1231

1232
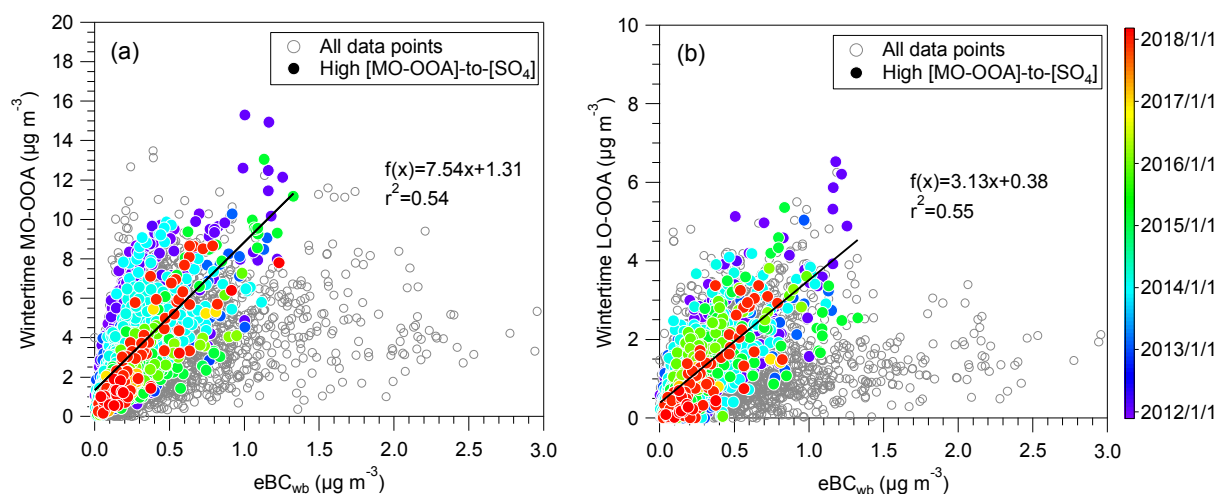
Figure 6. Correlations between SOA factors (MO-OOA and LO-OOA) with a BB-related tracer

(eBC$_{wb}$) during wintertime. The color-coded solid circle points (in a and b) are the data points

corresponding to high ratios of [MO-OOA]-to-[SO$_4$] (more than 8), for which the curve fits are

performed.

1238
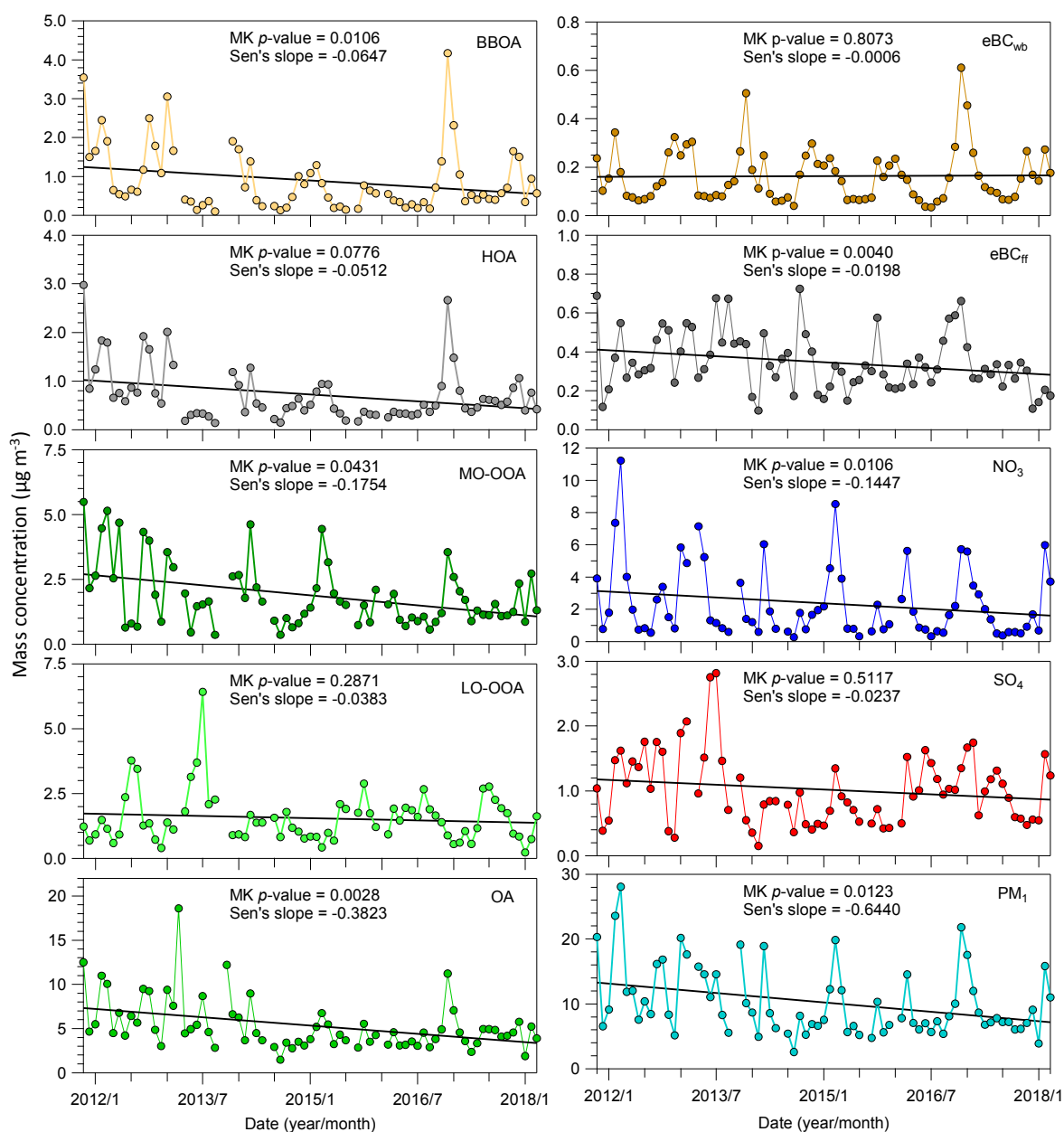
Figure 7. Temporal trends of monthly mass concentrations of different chemical speciation, including eBC$_{wb}$, eBC$_{ff}$, SO$_4$ (sulfate), NO$_3$ (nitrate), four OA factors, total OA, and total PM$_1$ (the sum of NR-PM$_1$ and eBC). The MK or seasonal MK testes associated with estimated Sen's slope (µg m^{-3} per year) were used for the trend analysis.

1239

1240

1241

1242

1243

1244
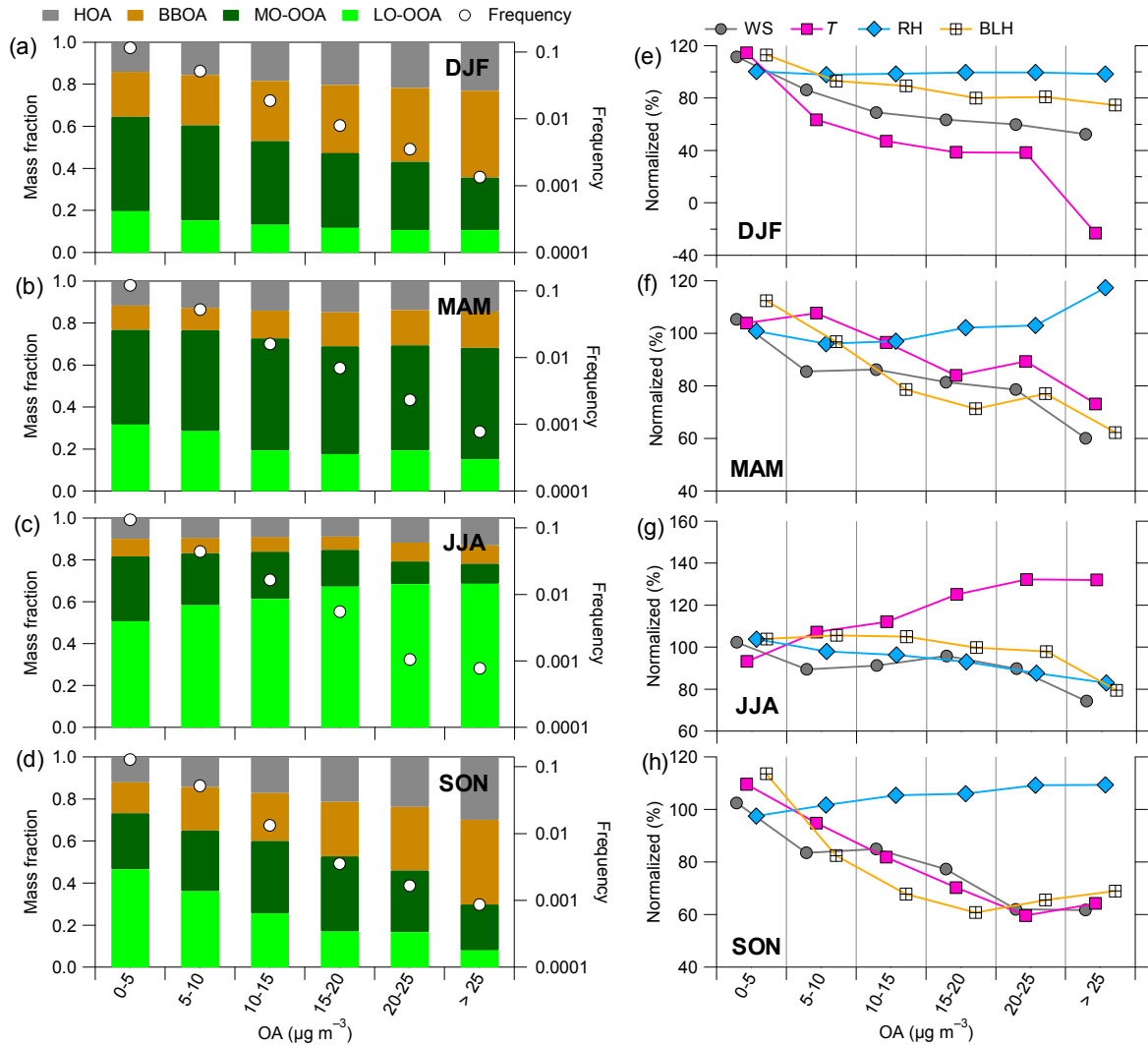
Figure 8. (a-d) mass fraction of OA factors and (e-h) meteorological parameters (i.e., WS, *T*, RH, and BLH) as a function of OA mass loadings in four seasons: winter (DJF), spring (MAM), summer (JJA), and fall (SON), along with frequency distributions (white circle points). The percent change of all meteorological parameters was normalized based on the average values over the 6[+]-years period considered here.

1245
1246
1247
1248
1249

1250

1251
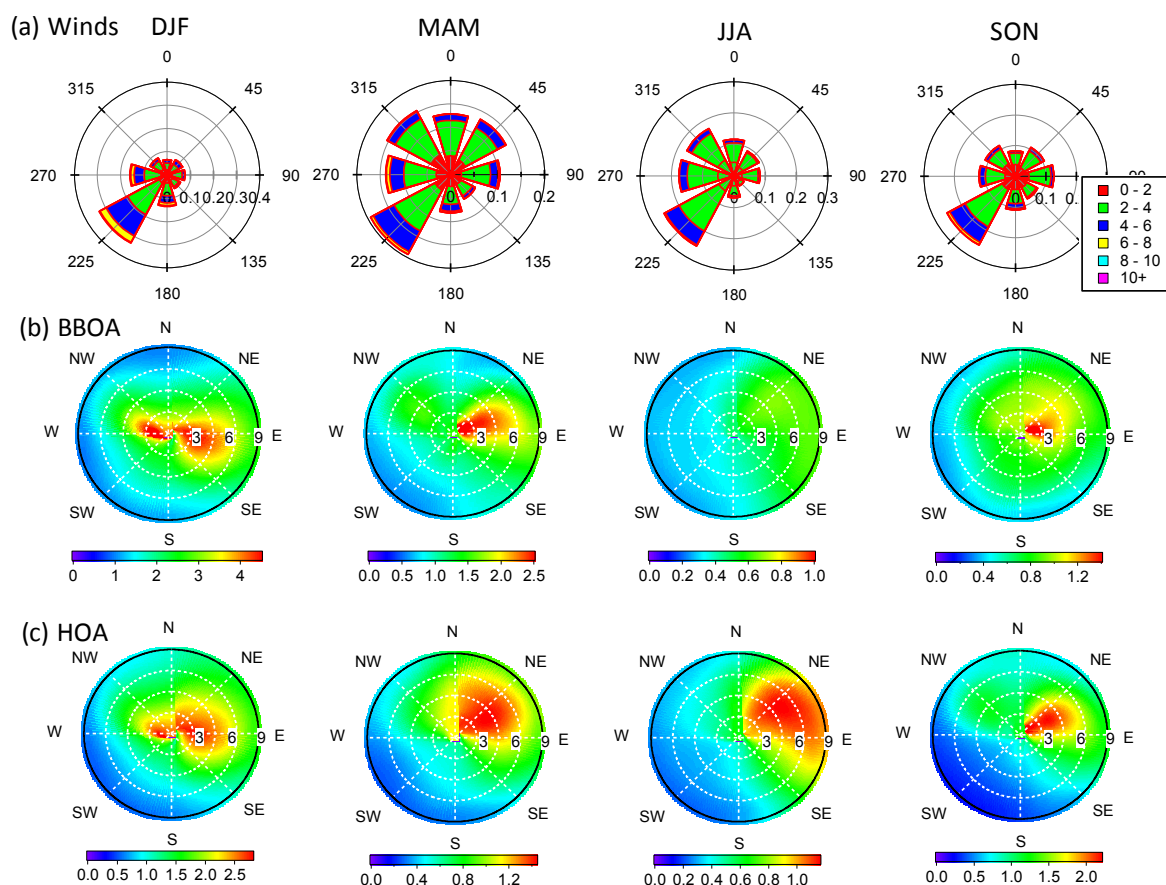
Figure 9. Seasonal wind dependence of POA factors. (a) Wind rose plots color-coded by wind

speed (m s^{-1}), and (b) BBOA and (c) HOA, color-coded by mass concentrations (µg m^{-3}).

1254

1255
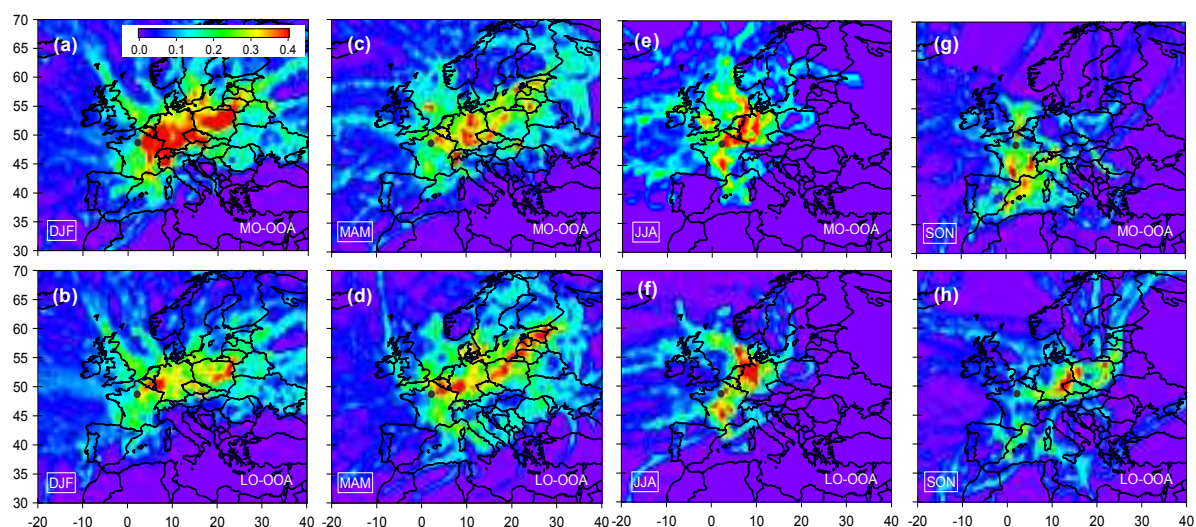
Figure 10. Maps for potential source origins of regional transports that may contribute to SOA (including MO-OOA and LO-OOA) burdens at SIRTA. Observed data points with wind speed (less than 4 m s^{-1}) and in the presence of precipitation events are filtered for the PSCF calculation. Black solid point in each plot presents the location of the sampling site.

1260